

# Electroweak corrections to squark–antisquark production at the LHC

---

## Wolfgang Hollik

*Max-Planck-Institut für Physik, Föhringer Ring 6, D-80805 München, Germany;*  
*Email: hollik@mpp.mpg.de*

## Jonas M. Lindert

*Physik-Institut, Universität Zürich, Wintherturerstrasse 190, CH-8057 Zürich, Switzerland; E-mail: lindert@physik.uzh.ch*

## Edoardo Mirabella\*

*Max-Planck-Institut für Physik, Föhringer Ring 6, D-80805 München, Germany;*  
*E-mail: mirabell@mpp.mpg.de*

## Davide Pagani

*Centre for Cosmology, Particle Physics and Phenomenology (CP3), Université Catholique de Louvain, B-1348 Louvain-la-Neuve, Belgium;*  
*E-mail: davide.pagani@uclouvain.be*

**ABSTRACT:** We present the calculation of the electroweak corrections for squark–antisquark pair production at the LHC within the Minimal Supersymmetric Standard Model. Taking into account all possible chirality and light-flavor configurations, we evaluate the NLO EW corrections, which are of  $\mathcal{O}(\alpha_s^2\alpha)$ , as well as the subleading tree-level contributions of  $\mathcal{O}(\alpha_s\alpha)$  and  $\mathcal{O}(\alpha^2)$ . Numerical results are presented for several scans in the SUSY parameter space and relevant differential distributions are investigated. The impact of the electroweak corrections is nonnegligible and strongly depends on the chirality configuration of the produced squarks. Our analysis includes a discussion of photon–gluon initiated processes with a focus on the impact of the corresponding large PDF uncertainties.

---

\*Now at Fleuchaus & Gallo Partnerschaft mbB, Patent- und Rechtsanwälte

---

## Contents

<b>1. Introduction</b>	<b>1</b>
<b>2. Calculation method</b>	<b>3</b>
<b>3. Numerical results</b>	<b>8</b>
3.1 PDF uncertainties in the gluon–photon channel	10
3.2 Inclusive cross sections	12
3.3 Differential distributions	15
<b>4. Conclusions</b>	<b>16</b>

---

## 1. Introduction

Supersymmetry (SUSY) [1] is one of the theoretically most appealing beyond -the-Standard-Model (BSM) scenarios. In particular, the minimal supersymmetric extension of the Standard Model (MSSM) [2–4] predicts a light scalar Higgs boson that is compatible with the resonance observed at the LHC experiments [5, 6]. Moreover, the MSSM naturally stabilizes the electroweak vacuum and, assuming R-parity conservation, provides also a dark matter candidate.

These features give to SUSY a central role in the BSM searches at the LHC. Within the MSSM the analyses of the first-run LHC data have investigated several final states and signatures [7, 8]. All the analyses found no significant deviation from SM predictions, setting limits on the SUSY spectrum. Still, the second run of the LHC, at higher energies and higher luminosity, will probe larger regions of the MSSM parameter space that are not excluded at the moment by experimental searches.

At the LHC, the production of a pair of colored SUSY particles ( $\tilde{q}\tilde{q}'$ ,  $\tilde{q}\tilde{q}'^*$ ,  $\tilde{g}\tilde{g}$ ,  $\tilde{g}\tilde{g}^{(*)}$ ) plays a crucial role in the context of direct searches; their cross sections are the largest among all the possible production mechanisms. The phenomenological relevance of this class of processes has triggered an extensive effort in improving the precision of their theoretical predictions. Not only the leading-order (LO) contributions [9–13], but also the complete set of next-to-leading order (NLO) QCD corrections [14–20] and most of the NLO electroweak (EW) corrections [21–33] are available in the literature. Approximate next-to-next-to-leading order (NNLO) QCD corrections to squark–antisquark production have been computed as well [34–37].

Besides fixed order calculations, the large corrections in the threshold region have been computed at the next-to-leading (NLL) [38–42] and next-to-next-to-leading (NNLL) [43–47] logarithmic accuracy. Effective field theory approaches allowed also for the resummation

of soft-gluon and Coulomb corrections [48–51]. Moreover, gluino and stop bound states have been studied [52, 53] and the bound-state effects in gluino–gluino and squark–gluino production have also been analyzed [54–56].

Also the squark and gluino decay rate is known at the NLO accuracy, including both QCD [57–59] and EW [60, 61] corrections. Phenomenological studies systematically including the NLO QCD corrections to the combined production and decays of squark–squark and stop–antistop pairs have been respectively performed in [18, 62] and [63, 64]. In [65, 66], the NLO QCD corrections to squark–squark and squark–antisquark production have been matched to parton showers.

From the experimental side, the lack of a signal from direct searches has increased the lower bounds on the masses of the supersymmetric particles, especially for those that are colored. In particular, the most stringent bounds have been set on light-flavor squarks and gluinos. For instance, assuming a simplified MSSM scenario with only the gluino and degenerate light-flavor squarks production with decay into a massless neutralino, the gluino (light-flavor squark) mass should be heavier than 1.4 TeV (1.6 TeV). Under the same hypotheses, degenerate light-flavor squarks and gluinos should be heavier than 1.8 TeV [67].

In these experimental analyses the simulation of the signal takes into account only part of the aforementioned higher-order corrections. In particular signal events are obtained by following [68], i.e., they are produced at LO accuracy and afterwards they are globally reweighted via the  $K$ -factors from the inclusive NLO+NLL QCD total cross section that is obtained from the codes `Prospino` [69] and `NLL-fast` [42]. The theoretical uncertainty affecting the signal is evaluated by varying both the parton distribution function (PDF) sets and the renormalization/factorization scale. It is worth to notice that this procedure does not account for the kinematical dependence of the higher-order contributions and for the significant impact of the NLO corrections to the decays of the produced particles [18, 62–64]. Moreover corrections of EW origin are completely ignored both in the evaluation of signal and in the estimation of the theoretical uncertainty. Since EW corrections naturally involve most of the MSSM particles via loop corrections, they formally depend on the specific scenario considered. For instance, a large mass gap between colored and uncolored particles may in principle enhance their effect beyond the percent level. In order to have under control the impact of higher-order corrections, it is necessary to explicitly check these effects and identify for which parameters EW corrections possibly show sizable dependencies.

In this paper we perform this type of analyses, focussing on the hadronic associate production of a light-flavor squark (a squark of the first two generations) together with a light-flavor antisquark,

$$PP \rightarrow \tilde{q}_\alpha \tilde{q}'_\beta^*, \quad (1.1)$$

where  $q, q' = u, d, c, s$ , while  $\alpha$  and  $\beta$  denote the chirality of the corresponding squark,  $\alpha, \beta = L, R$ . We compute the EW corrections to the processes (1.1) extending and completing the analysis of [26], which focused only on same-flavor, same-chirality squark–antisquark production,  $PP \rightarrow \tilde{q}_\alpha \tilde{q}_\alpha^*$ . Moreover, we present for this process the first phenomenological study combining NLO QCD and NLO EW corrections. Our study mainly focuses on the NLO corrections to the inclusive squark–antisquark production cross section, and it can

be directly used in experimental analyses to estimate the theoretical uncertainty related to the missing EW corrections. Additionally, the impact of the EW corrections on kinematic distributions for undecayed squarks is considered as well.

The outline of the paper is as follows. Section 2 describes the various partonic processes contributing up to  $\mathcal{O}(\alpha_s^2\alpha)$  and the strategy of the calculation. The numerical impact of the EW and QCD corrections are discussed in Section 3, followed by our conclusions in Section 4.

## 2. Calculation method

In our calculation we consider and treat independently all the possible light-flavor and chirality configurations for squark–antisquark pairs, as denoted in eq. (1.1). Since we treat quarks of the first two generations as massless, the squark chirality eigenstates are also the mass eigenstates, thus each squark–antisquark pair can separately be considered as a physical final state. In total, the possible two chirality/mass eigenstates for each of the four (anti)squark flavor ( $u, d, c, s$ ) lead to eight distinguished types of (anti)squarks and thus to sixty-four possible  $\tilde{q}_\alpha\tilde{q}_\beta^*$  squark–antisquark pairs.

For each one of these sixty-four final states the LO cross section is of  $\mathcal{O}(\alpha_s^2)$ . In our calculation, we take into account the complete set of NLO EW corrections, which are of  $\mathcal{O}(\alpha_s^2\alpha)$ , and all the contributions originating from tree-level diagrams only. The latter include the LO, but also  $\mathcal{O}(\alpha_s\alpha)$  contributions, which arise from the interference of  $\mathcal{O}(\alpha_s)$  and  $\mathcal{O}(\alpha)$  amplitudes, and  $\mathcal{O}(\alpha^2)$  contributions from  $\mathcal{O}(\alpha)$  squared amplitudes. With the term “EW corrections” we will in general indicate the sum of  $\mathcal{O}(\alpha_s^2\alpha)$ ,  $\mathcal{O}(\alpha_s\alpha)$  and  $\mathcal{O}(\alpha^2)$  contributions.

All these contributions are independently calculated for each one of the sixty-four final states. Thus, the masses of the eight different (anti)squarks can be treated as completely non-degenerate. In our phenomenological analyses of Section 3, we will include also NLO QCD corrections by the help of the code `Prospino` [69], which is based on the calculation in [16]. However, in order to obtain genuine NLO QCD corrections, the usage of `Prospino` and thus the evaluation of NLO QCD corrections will be performed only for degenerate squark masses and only at the level of inclusive cross sections.

In the following we describe the organization of the calculation of the EW corrections and we explain in detail how the different perturbative orders enter for the sixty-four final states. To this end, it is useful to identify classes of processes that share the same type of partonic initial states for the different perturbative order under consideration. Among the sixty-four final states we may distinguish five different classes of processes:

- **$\tilde{u}_L\tilde{u}_L^*$ -type** processes producing squarks with same flavor and chirality,

$$PP \rightarrow \tilde{u}_\alpha\tilde{u}_\alpha^*, \quad \tilde{d}_\alpha\tilde{d}_\alpha^*, \quad \tilde{c}_\alpha\tilde{c}_\alpha^*, \quad \tilde{s}_\alpha\tilde{s}_\alpha^*. \quad (2.1a)$$

- **$\tilde{u}_L\tilde{u}_R^*$ -type** processes producing squarks with same flavor and different chirality,

$$PP \rightarrow \tilde{u}_\alpha\tilde{u}_\beta^*, \quad \tilde{d}_\alpha\tilde{d}_\beta^*, \quad \tilde{c}_\alpha\tilde{c}_\beta^*, \quad \tilde{s}_\alpha\tilde{s}_\beta^*, \quad \alpha \neq \beta. \quad (2.1b)$$

Processes	Channels		
	$\mathcal{O}(\alpha_s)$	$\mathcal{O}(\alpha)$	$\mathcal{O}(\alpha_s^{1/2}\alpha^{1/2})$ $\gamma$ -ind.
$\tilde{u}_L\tilde{u}_L^*$ -type			
$\tilde{u}_L\tilde{c}_L^*$ -type			
$\tilde{u}_L\tilde{d}_L^*$ -type			
$\tilde{u}_L\tilde{u}_R^*$ and $\tilde{u}_L\tilde{s}_L^*$ -type			

Table 1: Representative tree-level diagrams for the different partonic subprocesses entering the various squark–antisquark production processes. The diagrams in red enter only if  $q = q'$ , while the diagram in blue contributes only if  $q$  and  $q'$  belong to the same  $SU(2)$  doublet. The quarks  $p_q$  and  $r_q$  are defined in eqs. (2.4).

- **$\tilde{\mathbf{u}}_L\tilde{\mathbf{c}}_L^*$ -type** processes producing two up-type or two down-type squarks with different flavor,

$$PP \rightarrow \tilde{u}_\alpha \tilde{c}_\beta^*, \tilde{c}_\alpha \tilde{u}_\beta^*, \tilde{d}_\alpha \tilde{s}_\beta^*, \tilde{s}_\alpha \tilde{d}_\beta^*. \quad (2.1c)$$

- **$\tilde{\mathbf{u}}_L\tilde{\mathbf{s}}_L^*$ -type** processes producing one up-type and one down-type squark of different families,

$$PP \rightarrow \tilde{u}_\alpha \tilde{s}_\beta^*, \tilde{s}_\alpha \tilde{u}_\beta^*, \tilde{d}_\alpha \tilde{c}_\beta^*, \tilde{c}_\alpha \tilde{d}_\beta^*. \quad (2.1d)$$

- **$\tilde{\mathbf{u}}_L\tilde{\mathbf{d}}_L^*$ -type** processes producing one up-type squark and one down-type squark of the same family,

$$PP \rightarrow \tilde{u}_\alpha \tilde{d}_\beta^*, \tilde{d}_\alpha \tilde{u}_\beta^*, \tilde{c}_\alpha \tilde{s}_\beta^*, \tilde{s}_\alpha \tilde{c}_\beta^*. \quad (2.1e)$$

This classification is based only on the technical aspects of the computation. In particular it does not consider the dependence of the partonic contributions on the chirality and the

flavor of the produced squarks, e.g.,  $\tilde{d}_R\tilde{d}_R^*$  production is considered to be a  $\tilde{u}_L\tilde{u}_L^*$ -type process. Therefore members of the same class entail numerically different contributions. For example, all necessary matrix elements for  $\tilde{d}_R\tilde{d}_R^*$  production can be obtained directly from  $\tilde{u}_L\tilde{u}_L^*$  matrix elements by flipping the chirality and SU(2) states. In general, a global flip of chiralities, families and/or SU(2) states project a specific squark–antisquark pair, and its corresponding matrix elements, into another one of the same class. In order to correctly perform such a flip, the Feynman rules for all interaction vertices are written in the most general form allowing for arbitrary chirality and SU(2) states. Correspondingly, for a specific chirality or flavor configuration within a given class individual diagrams might vanish. The presented classification allows for a dramatic reduction of the number of matrix elements that have to be practically computed.

In order to specify the structure of the EW corrections, for any partonic subprocess  $X$  we will denote the contribution of  $\mathcal{O}(\alpha_s^a\alpha^b)$  to the total hadronic cross section as  $\sigma_X^{a,b}$ . This notation can be easily generalized to any observable and differential distribution for the squark–antisquark system.

We start considering the contributions to the cross section from tree-level diagrams only. As already noted, these contributions can be of  $\mathcal{O}(\alpha_s^2)$ ,  $\mathcal{O}(\alpha_s\alpha)$  and  $\mathcal{O}(\alpha^2)$ . Since quark–antiquark initial states can produce a squark–antisquark pair with the same flavor configuration via a QCD or a EW gauge boson or gaugino in the t-channel, the amplitudes of  $\mathcal{O}(\alpha_s)$  and  $\mathcal{O}(\alpha)$  for  $q\bar{q}' \rightarrow \tilde{q}_\alpha\tilde{q}'_\beta^*$  are always present. The corresponding Feynman diagrams are shown for each class in the first two columns of Table 1. Consequentially,  $\mathcal{O}(\alpha_s^2)$  and  $\mathcal{O}(\alpha^2)$  cross sections are always nonzero for each squark–antiquark chiral and flavor configuration. On the contrary,  $\mathcal{O}(\alpha_s\alpha)$  cross sections can be zero, since the interference of  $\mathcal{O}(\alpha_s)$  and  $\mathcal{O}(\alpha)$  amplitudes can vanish in particular classes due to the color flow or chirality structure.

For this reason, it is convenient to separate the contribution  $\sigma_{q\bar{q}' \rightarrow \tilde{q}_\alpha\tilde{q}'_\beta^*}^{2,0}$  and  $\sigma_{q\bar{q}' \rightarrow \tilde{q}_\alpha\tilde{q}'_\beta^*}^{0,2}$  from all the others in the sum over all parton channels,

$$\begin{aligned}\sigma_{PP \rightarrow \tilde{q}_\alpha\tilde{q}'_\beta^*}^{2,0} &= \sigma_{q\bar{q}' \rightarrow \tilde{q}_\alpha\tilde{q}'_\beta^*}^{2,0} + \bar{\sigma}_{PP \rightarrow \tilde{q}_\alpha\tilde{q}'_\beta^*}^{2,0}, \\ \sigma_{PP \rightarrow \tilde{q}_\alpha\tilde{q}'_\beta^*}^{1,1} &= \bar{\sigma}_{PP \rightarrow \tilde{q}_\alpha\tilde{q}'_\beta^*}^{1,1}, \\ \sigma_{PP \rightarrow \tilde{q}_\alpha\tilde{q}'_\beta^*}^{0,2} &= \sigma_{q\bar{q}' \rightarrow \tilde{q}_\alpha\tilde{q}'_\beta^*}^{0,2} + \bar{\sigma}_{PP \rightarrow \tilde{q}_\alpha\tilde{q}'_\beta^*}^{0,2}.\end{aligned}\tag{2.2}$$

In eq. (2.2) all the process-dependent contributions are included in the barred quantities  $\bar{\sigma}_{PP \rightarrow \tilde{q}_\alpha\tilde{q}'_\beta^*}^{a,b}$ . The specific structure of  $\bar{\sigma}_{PP \rightarrow \tilde{q}_\alpha\tilde{q}'_\beta^*}^{a,b}$  for each one of the five classes is listed in the following,

$$\tilde{u}_L\tilde{u}_L^*\text{-type:}\quad \left\{ \begin{aligned}\bar{\sigma}_{PP \rightarrow \tilde{q}_\alpha\tilde{q}'_\alpha^*}^{2,0} &= \sigma_{g\bar{g} \rightarrow \tilde{q}_\alpha\tilde{q}'_\alpha^*}^{2,0} + \sum_{q'' \neq q} \sigma_{q''\bar{q}'' \rightarrow \tilde{q}_\alpha\tilde{q}'_\alpha^*}^{2,0} \\ \bar{\sigma}_{PP \rightarrow \tilde{q}_\alpha\tilde{q}'_\alpha^*}^{1,1} &= \sigma_{q\bar{q} \rightarrow \tilde{q}_\alpha\tilde{q}'_\alpha^*}^{1,1} + \sigma_{g\gamma \rightarrow \tilde{q}_\alpha\tilde{q}'_\alpha^*}^{1,1} \\ \bar{\sigma}_{PP \rightarrow \tilde{q}_\alpha\tilde{q}'_\alpha^*}^{0,2} &= \sum_{q'' \neq q} \sigma_{q''\bar{q}'' \rightarrow \tilde{q}_\alpha\tilde{q}'_\alpha^*}^{0,2}\end{aligned}\right.,\tag{2.3a}$$

$$\tilde{u}_L \tilde{c}_L^* \text{-type:} \quad \begin{cases} \bar{\sigma}_{PP \rightarrow \tilde{q}_\alpha \tilde{q}'_\beta^*}^{2,0} = 0 \\ \bar{\sigma}_{PP \rightarrow \tilde{q}_\alpha \tilde{q}'_\beta^*}^{1,1} = 0 \\ \bar{\sigma}_{PP \rightarrow \tilde{q}_\alpha \tilde{q}'_\beta^*}^{0,2} = \sigma_{p_q \bar{p}_{q'} \rightarrow \tilde{q}_\alpha \tilde{q}'_\beta^*}^{0,2} \end{cases}, \quad (2.3b)$$

$$\tilde{u}_L \tilde{d}_L^* \text{-type:} \quad \begin{cases} \bar{\sigma}_{PP \rightarrow \tilde{q}_\alpha \tilde{q}'_\beta^*}^{2,0} = 0 \\ \bar{\sigma}_{PP \rightarrow \tilde{q}_\alpha \tilde{q}'_\beta^*}^{1,1} = \sigma_{q\bar{q}' \rightarrow \tilde{q}_\alpha \tilde{q}'_\beta^*}^{1,1} \\ \bar{\sigma}_{PP \rightarrow \tilde{q}_\alpha \tilde{q}'_\beta^*}^{0,2} = \sigma_{r_q \bar{r}_{q'} \rightarrow \tilde{q}_\alpha \tilde{q}'_\beta^*}^{0,2} \end{cases}, \quad (2.3c)$$

$$\tilde{u}_L \tilde{u}_R^* \text{ and } \tilde{u}_L \tilde{s}_L^* \text{-type:} \quad \begin{cases} \bar{\sigma}_{PP \rightarrow \tilde{q}_\alpha \tilde{q}'_\beta^*}^{2,0} = 0 \\ \bar{\sigma}_{PP \rightarrow \tilde{q}_\alpha \tilde{q}'_\beta^*}^{1,1} = 0 \\ \bar{\sigma}_{PP \rightarrow \tilde{q}_\alpha \tilde{q}'_\beta^*}^{0,2} = 0 \end{cases}. \quad (2.3d)$$

In the previous equations the quark  $p_q$  denotes the SU(2) partner of the quark  $q$ ,

$$p_u = d, \quad p_d = u, \quad p_c = s, \quad p_s = c, \quad (2.4a)$$

while the quark  $r_q$  is defined as follows,

$$r_u = c, \quad r_d = s, \quad r_c = u, \quad r_s = d, \quad (2.4b)$$

i.e.  $r_q$  and  $q$  are same-charge quarks belonging to different generations. All these contributions have been successfully checked at numerical level against both **Madgraph** [70] and **Prospino** [69].

The NLO EW corrections, i.e. the  $\mathcal{O}(\alpha_s^2 \alpha)$  contribution, constitute the original computation of this paper. Besides virtual corrections, this order receives contributions also from the real radiation of gluons, photons and (anti-)quarks. The  $\mathcal{O}(\alpha_s^2 \alpha)$  corrections to the cross section can be written as follows,

$$\begin{aligned} \sigma_{PP \rightarrow \tilde{q}_\alpha \tilde{q}'_\beta^*}^{2,1} &= \sigma_{q\bar{q}' \rightarrow \tilde{q}_\alpha \tilde{q}'_\beta^*}^{2,1} + \sigma_{q\bar{q}' \rightarrow \tilde{q}_\alpha \tilde{q}'_\beta^* g}^{2,1} + \sigma_{q\bar{q}' \rightarrow \tilde{q}_\alpha \tilde{q}'_\beta^* \gamma}^{2,1} \\ &\quad + \sigma_{qg \rightarrow \tilde{q}_\alpha \tilde{q}'_\beta^* q'}^{2,1} + \sigma_{\bar{q}'g \rightarrow \tilde{q}_\alpha \tilde{q}'_\beta^* \bar{q}}^{2,1} + \bar{\sigma}_{PP \rightarrow \tilde{q}_\alpha \tilde{q}'_\beta^*}^{2,1}. \end{aligned} \quad (2.5)$$

Again, with the barred quantity  $\bar{\sigma}_{PP \rightarrow \tilde{q}_\alpha \tilde{q}'_\beta^*}^{2,1}$  we denote the set of initial states that are class-dependent. The term  $\bar{\sigma}_{PP \rightarrow \tilde{q}_\alpha \tilde{q}'_\beta^*}^{2,1}$  is nonzero only for  $\tilde{u}_L \tilde{u}_L^*$ -type processes, i.e.,

$$\begin{aligned} \tilde{u}_L \tilde{u}_L^* \text{-type:} \quad \bar{\sigma}_{PP \rightarrow \tilde{q}_\alpha \tilde{q}'_\beta^*}^{2,1} &= \sigma_{gg \rightarrow \tilde{q}_\alpha \tilde{q}'_\beta^*}^{2,1} + \sigma_{gg \rightarrow \tilde{q}_\alpha \tilde{q}'_\beta^* \gamma}^{2,1} \\ &\quad + \sum_{q'' \neq q} \left( \sigma_{q'' \bar{q}'' \rightarrow \tilde{q}_\alpha \tilde{q}'_\beta^*}^{2,1} + \sigma_{q'' \bar{q}'' \rightarrow \tilde{q}_\alpha \tilde{q}'_\beta^* g}^{2,1} \right. \\ &\quad \left. + \sigma_{q'' \bar{q}'' \rightarrow \tilde{q}_\alpha \tilde{q}'_\beta^* \gamma}^{2,1} + \sigma_{q'' g \rightarrow \tilde{q}_\alpha \tilde{q}'_\beta^* q''}^{2,1} + \sigma_{\bar{q}'' g \rightarrow \tilde{q}_\alpha \tilde{q}'_\beta^* \bar{q}''}^{2,1} \right), \end{aligned} \quad (2.6a)$$

$$\text{other processes:} \quad \bar{\sigma}_{PP \rightarrow \tilde{q}_\alpha \tilde{q}'_\beta^*}^{2,1} = 0. \quad (2.6b)$$

At the same order of perturbation theory, i.e. at  $\mathcal{O}(\alpha_s^2\alpha)$  in principle also NLO QCD corrections to the  $\mathcal{O}(\alpha_s\alpha)$  photon-induced squark–antisquark production enter. We do not consider these contribution here.

The NLO EW corrections (2.5) depend on the full set of the MSSM parameters and have been evaluated by using `FeynArts` [71, 72], `FormCalc` [72, 73] and, for the evaluation of the one-loop integrals, `LoopTools` [72]. The cancellations of the ultraviolet divergences involves both  $\mathcal{O}(\alpha_s)$  and  $\mathcal{O}(\alpha)$  one-loop renormalization and has been extensively described in [26, 31]. Infrared singularities (IR) are regularized by introducing a small mass for the photon and the gluon, while quark masses are kept as regulators for the collinear singularities. In the processes considered, the IR singularities of gluonic origin are Abelian-like and can be safely treated by using mass regularization. Infrared and collinear singularities are handled by the double cut-off phase-space-slicing method [74–76], along the lines of [31]. The initial-state collinear singularities of gluonic (photonic) origin are factorized and absorbed in the parton distribution functions by using the  $\overline{\text{MS}}$  (DIS) scheme. We carefully checked that, on the level of inclusive cross sections and of individual distributions, all our numerical results do not depend on the two phase-space slicing parameters and on the fictitious gluon and light-flavor quark masses.

The amplitudes for partonic processes with (anti)quark–gluon in the initial state may exhibit an internal gluino, neutralinos or charginos that can go on-shell. This happens when one of these particles is heavier than one of the (anti)squarks produced. However, the corresponding Breit-Wigner distributions appear only at  $\mathcal{O}(\alpha_s^3)$  or  $\mathcal{O}(\alpha_s\alpha^2)$ , but not at  $\mathcal{O}(\alpha_s^2\alpha)$ . Thus, similarly to the squark-squark production case [26, 31], in NLO EW corrections these singularities do not correspond to a physical resonance. In order to avoid numerical instabilities, the poles have been regularized by including the width for the resonant particle in the corresponding propagators. Practically, the width plays the role of a regulator parameter, numerical results do not depend on its value.

Technical details of our calculation have already been extensively discussed in [26], where NLO EW corrections were calculated for the  $\tilde{u}_L\tilde{u}_L^*$ -type processes only.

The NLO QCD corrections, of  $\mathcal{O}(\alpha_s^3)$ , depend only on the mass of the squarks and of the gluino and have been computed in [16]. For the phenomenological studies of section 3, we evaluated them for total cross sections in the degenerate squark-mass case with the code `Prospino` [69]. For completeness we show the general structure of the NLO QCD contributions, using the same notation adopted in eqs. (2.5) and (2.6) for NLO EW corrections:

$$\begin{aligned} \sigma_{PP\rightarrow\tilde{q}_\alpha\tilde{q}'_\beta^*}^{3,0} &= \sigma_{q\bar{q}'\rightarrow\tilde{q}_\alpha\tilde{q}'_\beta^*}^{3,0} + \sigma_{q\bar{q}'\rightarrow\tilde{q}_\alpha\tilde{q}'_\beta^*g}^{3,0} + \sigma_{qg\rightarrow\tilde{q}_\alpha\tilde{q}'_\beta^*q'}^{3,0} \\ &+ \sigma_{\bar{q}'g\rightarrow\tilde{q}_\alpha\tilde{q}'_\beta^*\bar{q}}^{3,0} + \bar{\sigma}_{PP\rightarrow\tilde{q}_\alpha\tilde{q}'_\beta^*}^{3,0}. \end{aligned} \quad (2.7)$$

Also in this case, the barred quantity  $\bar{\sigma}_{q'g\rightarrow\tilde{q}_\alpha\tilde{q}'_\beta^*\bar{q}}^{3,0}$  depends on the flavor and the chirality of the final states:

$$\tilde{u}_L\tilde{u}_L^*\text{-type:} \quad \bar{\sigma}_{PP\rightarrow\tilde{q}_\alpha\tilde{q}'_\alpha^*}^{3,0} = \sigma_{gg\rightarrow\tilde{q}_\alpha\tilde{q}'_\alpha^*}^{3,0} + \sigma_{gg\rightarrow\tilde{q}_\alpha\tilde{q}'_\alpha^*g}^{3,0} + \sum_{q''\neq q} \left( \sigma_{q''\bar{q}''\rightarrow\tilde{q}_\alpha\tilde{q}'_\alpha^*}^{3,0} \right)$$



$$+ \sigma_{q''\bar{q}''\rightarrow\tilde{q}_\alpha\tilde{q}_\alpha^*g}^{3,0} + \sigma_{q''g\rightarrow\tilde{q}_\alpha\tilde{q}_\alpha^*q''}^{3,0} + \sigma_{\bar{q}''g\rightarrow\tilde{q}_\alpha\tilde{q}_\alpha^*\bar{q}''}^{3,0} \Big), \quad (2.8a)$$

$$\text{other processes: } \bar{\sigma}_{PP\rightarrow\tilde{q}_\alpha\tilde{q}_\beta^*}^{3,0} = 0. \quad (2.8b)$$

### 3. Numerical results

The results presented in this paper are obtained for a hadronic center-of-mass energy of  $\sqrt{S} = 13$  TeV. The numerical evaluation of the hadronic cross sections has been performed by using the `NNPDF2.3QED.mc` PDF set [77], which includes the photon PDF and LO QED effects in the evolution of all the PDF members. Moreover, this set of positive-definite PDFs provides an excellent description of all hard scattering data [78] avoiding the negative cross sections for high-mass particle production described in [79].

The relevant Standard Model input parameters are taken from [80] and, consistently with the specific PDF set used, we set  $\alpha_s(m_Z) = 0.119$  in the numerical evaluations. Fermions of the first two generations are considered as massless. All the MSSM masses and couplings are determined by eleven independent TeV-scale parameters,

$$m_{A_0}, \quad \tan\beta, \quad X_t, \quad \mu, \quad M_2, \quad m_{\tilde{g}}, \quad M_{\tilde{q},L}, \quad M_{\tilde{q},R}, \quad M_{\tilde{\ell}}, \quad M_{\tilde{q}_3}, \quad M_{\tilde{\ell}_3}. \quad (3.1)$$

where, for the soft-breaking sfermion-mass parameters the relations

$$\begin{aligned} M_{\tilde{t},L/R} &= M_{\tilde{b},L/R} = M_{\tilde{q}_3}, & M_{\tilde{f},L/R} &= M_{\tilde{q},L/R}, & (f = u, d, c, s), \\ M_{\tilde{\tau},L/R} &= M_{\tilde{\nu}_\tau,L} = M_{\tilde{\ell}_3}, & M_{\tilde{f},L/R} &= M_{\tilde{\nu}_f,L} = M_{\tilde{\ell}}, & (f = e, \mu), \end{aligned} \quad (3.2a)$$

are assumed, and the bino mass  $M_1$  and the sfermion trilinear couplings are set to

$$M_1 = \frac{5 \sin^2 \theta_W}{3 \cos^2 \theta_W} M_2, \quad A_t = X_t - \frac{\mu}{\tan \beta}, \quad A_f = 0, \quad (f = e, \mu, \tau, u, d, c, s, b). \quad (3.2b)$$

In eq. (3.2b),  $M_1$  is obtained from gaugino-mass unification at the GUT scale. The physical spectrum and all the Feynman rules are derived from this parameter set by using tree-level relations. The only exception is the physical mass of the Higgs bosons, which is computed with the help of `FeynHiggs 2.10` [81–85].

In order to study both degenerate and non-degenerate scenarios, in the numerical discussion we will consider particular *slopes* of the  $(M_{\tilde{q},L}, M_{\tilde{q},R})$  plane, parametrized in terms of a mass  $M_{\tilde{q}}$  as follows (see also Fig. 1):

$$\begin{aligned} \text{slope } S_1 : & \quad (M_{\tilde{q},L}, M_{\tilde{q},R}) = (1, 1) \cdot M_{\tilde{q}}, \\ \text{slope } S_2 : & \quad (M_{\tilde{q},L}, M_{\tilde{q},R}) = (1, 2) \cdot M_{\tilde{q}}, \\ \text{slope } S_3 : & \quad (M_{\tilde{q},L}, M_{\tilde{q},R}) = (2, 1) \cdot M_{\tilde{q}}, \\ \text{slope } S_4 : & \quad (M_{\tilde{q},L}, M_{\tilde{q},R}) = (M_{\tilde{q}}, 1500 \text{ GeV}), \\ \text{slope } S_5 : & \quad (M_{\tilde{q},L}, M_{\tilde{q},R}) = (1500 \text{ GeV}, M_{\tilde{q}}). \end{aligned} \quad (3.3)$$

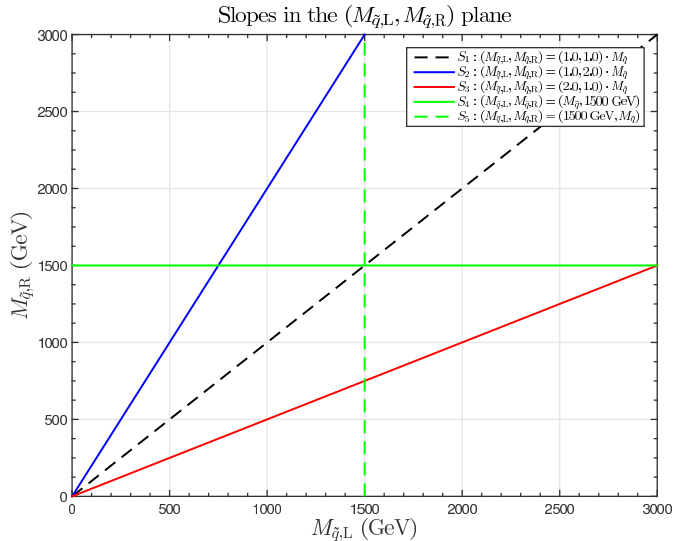


Figure 1: Slopes in the  $(M_{\tilde{q},L}, M_{\tilde{q},R})$  plane.

The slope  $S_1$  represents the degenerate case, whereas the other slopes correspond to different possible non-degenerate spectra. The motivation for considering non-degenerate scenarios is twofold. First, EW corrections depend on the chiralities of the produced particles. Thus, a mass gap between the different-chirality squarks is expected to modify the impact of EW corrections on the inclusive cross section for squark–antisquark production. Second, squarks of different chiralities may be experimentally distinguishable by their different decay products [62]. This is already relevant for the degenerate case<sup>1</sup> and plays an even more important role in case of large mass gaps, where the production of heavy states is suppressed and the experimental signature is determined by the decays of the lighter states.

In order to identify the dependence of the cross sections on the chirality of the produced (anti-)squarks, we will consider four different classes of final states:

- “LL” : production of a left-handed squark and a left-handed antisquark,
- “RR” : production of a right-handed squark and a right-handed antisquark,
- “LR+RL” : production of a squark and an antisquark with different chiralities,
- “incl.” : inclusive production of a squark–antisquark pair,

where the inclusive production is by definition given by the sum of all the final states in the “LL”, “RR” and “LR+RL” classes. Depending on the class and the point of the slope considered, the masses of a given squark–antisquark pair can be considerably different.

<sup>1</sup>Experimental analyses typically assume simplified models, where all the squarks decay directly into the lightest neutralinos. Allowing for different decays, very different signatures would emerge from left- and right-handed squarks. The corresponding bounds from direct searches would be consequentially modified.

As a general approach, we set the factorization scale  $\mu_F$  and the renormalization scale  $\mu_R$  equal to the average of the mass of the produced particles,  $\mu_F = \mu_R = (m_{\tilde{q}_\alpha} + m_{\tilde{q}'_\beta})/2$ , independently for each final state. It is worth to note that each one of the classes of processes in eq. (2.1) can in general contribute to LL, RR and LR+RL production. The only exceptions are  $\tilde{u}_L\tilde{u}_L^*$ -type processes, which do not contribute to LR+RL production, and  $\tilde{u}_L\tilde{u}_R^*$ -type processes which do not contribute to LL and RR production.

In the numerical results we will refer to any contribution either specifying explicitly its perturbative order (and partonic initial-state) or using the following standard notation:

- “LO” refers to  $\mathcal{O}(\alpha_s^2)$  contributions,
- “NLO QCD” refers to the sum of  $\mathcal{O}(\alpha_s^2)$  and  $\mathcal{O}(\alpha_s^3)$  contributions,
- “EW corr.” refers to the corrections of EW origin, i.e. to the sum of  $\mathcal{O}(\alpha_s\alpha)$ ,  $\mathcal{O}(\alpha^2)$  and  $\mathcal{O}(\alpha_s^2\alpha)$  contributions,
- “EW corr. (no  $g\gamma$ )” refers to the EW corrections *without* the contribution of the  $g\gamma$  channel.

Before presenting our numerical results, we want to comment on the choice and the motivations of presenting EW corrections with and without  $\mathcal{O}(\alpha_s\alpha)$  contributions from the  $g\gamma$  initial state.

### 3.1 PDF uncertainties in the gluon–photon channel

Direct production of massive particles, i.e. with masses above 1 TeV, probes PDFs at large Bjorken- $x$ , where they are poorly constrained by experimental data and exhibit large uncertainties. In the case of the direct production of 1 TeV (2 TeV) squark–antisquark pairs, e.g., the intrinsic uncertainties on the gluon and the quark PDFs lead to an uncertainty on the total NLO QCD cross section of the order of 4% (17%) [79]. EW corrections originate in general from processes with the same initial states of those from QCD corrections. Thus, the uncertainty on the total cross section induced by intrinsic PDF uncertainties from EW corrections is expected to be a fraction of the analogue contribution from the NLO QCD cross section.

An important exception in our calculation is the  $\mathcal{O}(\alpha_s\alpha)$  contribution from gluon–photon initial state, which appears in same-flavor same-chirality squark–antisquark production ( $\tilde{u}_L\tilde{u}_L^*$ -type processes). This initial state contributes to the EW corrections, but it does not contribute to LO cross sections and NLO QCD corrections. At  $\mathcal{O}(\alpha_s\alpha)$ , the only MSSM parameters entering the cross sections in the  $g\gamma$  channel are the masses of squarks and the gluino. Moreover, the photon PDF in NNPDF2.3QED is affected by large uncertainties [77], which have to be taken into account to correctly identify the impact of higher-order corrections [86, 87]. For this reason, before discussing the effect of EW corrections, we consider the PDF uncertainties arising from  $g\gamma$ -induced production and we describe their impact on our calculation and phenomenological studies. Here, we do not want to perform a complete analysis on the effects of PDF uncertainties from EW

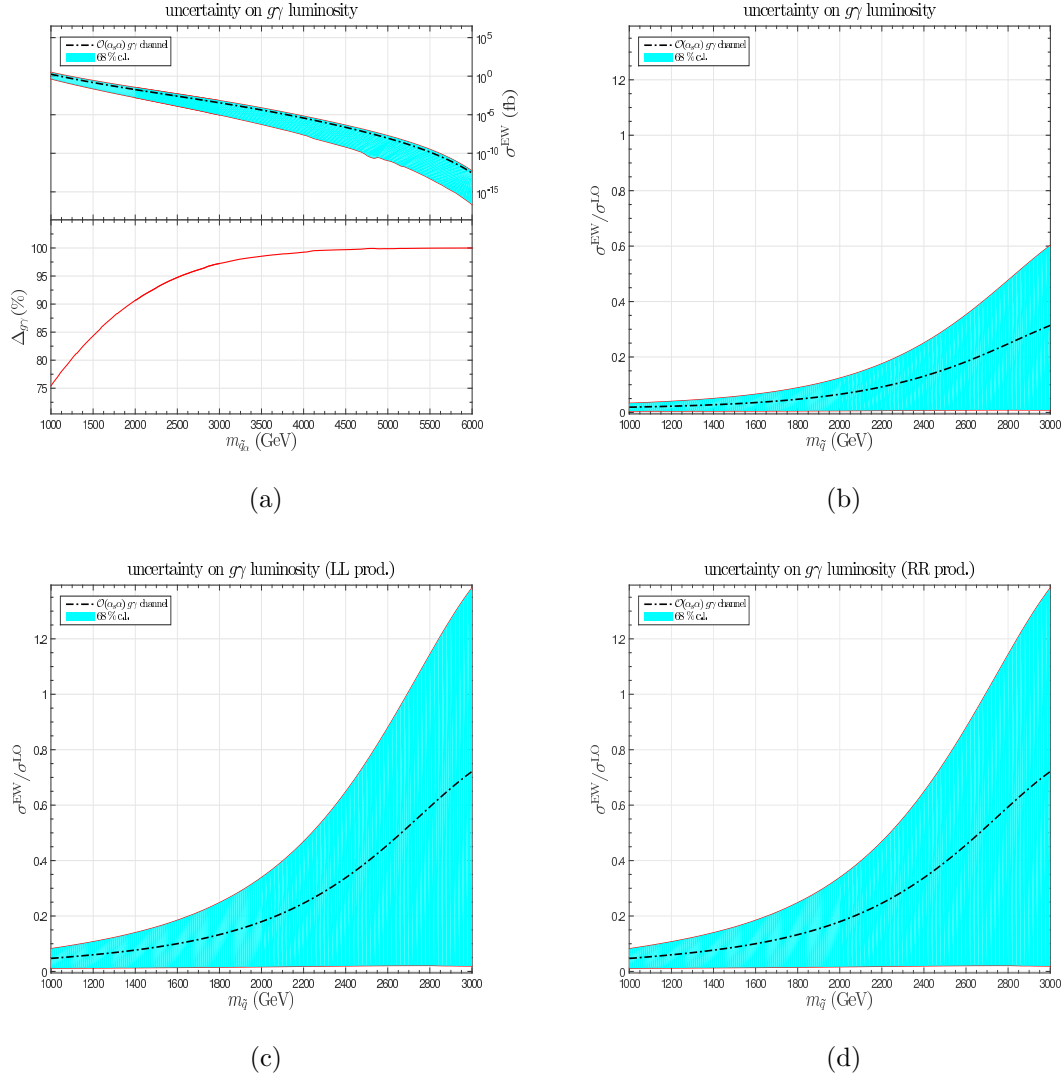


Figure 2: Absolute and relative contributions of the photon–gluon channel to the total hadronic cross section. Central values (black dash-dotted lines) and PDF uncertainties (blue bands) are plotted as function of a common squark mass  $m_{\tilde{q}}$  ( $m_{\tilde{g}} = 1500$  GeV). In panel (a)  $\Delta_{g\gamma \rightarrow \tilde{q}_\alpha \tilde{q}_\alpha^*}$  denotes the ratio between the PDF uncertainties of the cross section of the  $g\gamma$  channel and its absolute central value.

corrections<sup>2</sup>, instead we want to show how the evaluation of photon-induced production without PDF uncertainty can give qualitatively misleading results in the context of TeV-scale supersymmetric-particle production.

Fig. 2(a) depicts the contribution of the  $g\gamma$ -channel to squark–antisquark production as a function of the common mass of the produced squarks,  $m_{\tilde{q}}$  (degenerate case). The blue band around the central value (black solid line) corresponds to the PDF 68% c.l.

<sup>2</sup>This kind of study is typically not done even for SM processes. In case of discovery, it can be easily performed if it is necessary.

$m_{A_0}$	700 GeV	$\tan \beta$	20
$X_t$	$2M_{\tilde{q}_3}$	$\mu$	350 GeV
$M_2$	350 GeV	$m_{\tilde{g}}$	1500 GeV
$M_{\tilde{q},L}$	1500 GeV	$M_{\tilde{q},R}$	1500 GeV
$M_{\tilde{q}_3}$	500 GeV	$M_{\tilde{t}_3}$	1000 GeV
$M_{\tilde{\ell}}$	500 GeV		

Table 2: Default parameters within our eleven-parameter phenomenological MSSM.

error computed along the lines of [79]. In particular, since the photon PDF is positive by construction, replicas distribute in a very non-gaussian way. The 68% c.l. error around the central value corresponds to the symmetric error that includes 68 of the 100 results given by the different PDF replica from NNPDF2.3QED. In the lower panel, we plot as function of  $m_{\tilde{q}}$  the value of  $\Delta_{g\gamma}$ , which is defined as the ratio of the 68% c.l. error and the central value for the  $g\gamma$ -channel. As expected, the PDF uncertainty is very large. It ranges from 75% at  $m_{\tilde{q}} = 1$  TeV to almost 100% at  $m_{\tilde{q}} \geq 4$  TeV. Confronted with such a huge uncertainty it has to be understood that for heavy squarks the contribution from the  $g\gamma$ -channel is compatible both, with zero and the double of its central value. In a new version of NNPDF or in another future set of PDFs with QED evolution the size of the error could be very different. Thus, it is wise to keep the  $g\gamma$ -channel always as a separate contribution to the overall EW corrections.

The importance of keeping this term separate is even more evident when its size is compared to that of the LO cross section. An illustrative example may be found in Fig. 2(b), which shows the impact of the  $g\gamma$  channel relative to the leading order contribution, computed assuming  $m_{\tilde{g}} = 1500$  GeV. In the following we will focus on the productions of squark with masses below 2500 GeV, where the  $g\gamma$  channel is supposed to be smaller than 30% of the LO cross-section. This mass range will be probed by Run-II of the LHC [88].

Actually, the relative contribution of the  $g\gamma$  channel to the overall squark–antisquark production cross section is diluted by the “LR+RL” processes, which do not involve the  $g\gamma$  initial state. In the case of only LL or RR production, which do include the  $g\gamma$  initial-state contribution from  $\tilde{u}_L\tilde{u}_L^*$ -type processes, the impact of the photon PDF uncertainty is even more important, cfr. Figs. 2(c) and 2(d). With  $m_{\tilde{q}} = 2.5$  TeV, the  $g\gamma$  channel can induce corrections from zero up to 80% of the LO results. Clearly, this means that the precise contribution from the  $g\gamma$  channel is largely unknown, but it is potentially large. Conversely, without taking into account PDF uncertainties, one would be tempted to claim large effects of order 40% from photon-induced EW corrections. In the following discussion, we will not show the uncertainty band of the  $g\gamma$  channel. However, as general rule, one has to bare in mind an  $\mathcal{O}(100\%)$  uncertainty is always associated to its contribution.

### 3.2 Inclusive cross sections

For our numerical evaluation we consider the benchmark scenario defined in Table 2, which is a slight modification of the “light-stop” scenario defined in [89]. Starting from

this scenario we perform various one-dimensional scans, by varying the parameters in the list (3.1). Specifically, we considered scans over  $M_2$ ,  $m_{\tilde{q}}$ ,  $\mu$ ,  $\tan\beta$  and five different slopes in the  $(M_{\tilde{q},L}, M_{\tilde{q},R})$  plane, which have been defined in (3.3). Since we always consider  $M_{\tilde{q},L/R} > 1$  TeV, the soft breaking parameter  $M_{\tilde{q},L/R}$  can be safely considered as equal to the physical masses  $m_{\tilde{q},L/R}$ .<sup>3</sup> The regions considered in the scans are within the limits from the Higgs sector, i.e. they exhibit a Higgs-state close to the observed one, with couplings compatible with the observed rates in the Higgs search channels. The compatibility between the scenarios and the experimental results has been checked by using the codes `HiggsBounds` [90–93] and `HiggsSignals` [94], by following the procedure described in [33].

The results of the scans are shown in Figures 4–9. Since the scans over  $\mu$  and  $\tan\beta$  show that the total cross section is very insensitive to their values, we did not include them here. Each figure collects six plots related to a particular scan. Plot (a) shows the LO and NLO cross section predictions, inclusive over the sixty-four squark–antisquark pairs. In the lower panel of plot (a) we show the size of the corresponding relative corrections to the LO result. NLO QCD corrections are included only for degenerate squarks. The plot (b) shows the contributions of the individual channels and perturbative orders to the relative EW corrections and their sum. Thus, the blue line in plot (b) and the lower panel of plot (a) refer to the same quantity. Plot (c) shows the LO contributions of LL, RR, LR+RL processes and their sum; in the lower panel we display the relative EW corrections for each one of these classes. Panels (d), (e) and (f) respectively show the same kind of plot depicted in panels (b), but for the individual cases of LL, RR and LR+RL squark–antisquark production.

### Degenerate squark masses

**Slope S<sub>1</sub>**: Fig. 3 corresponds to the case of degenerate squarks, showing the dependence of squark–antisquark production on the common mass  $M_{\tilde{q}}$  of all light flavor squarks. The inclusive cross section varies over two orders of magnitude in the considered mass range. The QCD corrections vary from 50% to 70% as  $M_{\tilde{q}}$  varies from 1000 to 2500 GeV. The relative size of the total EW corrections increases with  $M_{\tilde{q}}$ , and Fig. 3(b) clearly shows that the total amount of the EW corrections is the result of substantial cancellations among the different channels. This cancellation may be jeopardized by the photon PDF uncertainty, since the  $g\gamma$ -channel (with its large uncertainties) has a large impact on the total size of the EW corrections, as can be seen from the comparison of red and blue lines in the lower panel of Fig. 3(a). Looking at the different chirality combinations separately, in the case of LL production, mutual cancellations among the various channels keep the total EW corrections small in the entire  $M_{\tilde{q}}$  range. On the contrary, in RR production the total EW corrections are positive and increase as  $M_{\tilde{q}}$  increases. However, without the (possibly) large positive  $g\gamma$ -channel the EW corrections are negative in the entire considered mass range, and they reach  $-20\%$  ( $-5\%$ ) for  $M_{\tilde{q}} = 2500$  GeV for LL(RR) production. The total EW contributions to LR+RL production, which gives the largest part of the “incl.” cross

---

<sup>3</sup>The physical masses are given by  $m_{\tilde{q},L/R} \simeq M_{\tilde{q},L/R} \left( 1 + \mathcal{O}\left(\frac{m_Z^2}{M_{\tilde{q},L/R}^2}\right) \right)$ . Thus, when e.g.  $M_{\tilde{q},L/R} = 1/1.5/2$  TeV, the physical mass and the soft mass parameters are equal at the 0.8/0.4/0.2% level.

section (see Fig. 3(c)), depend mildly on  $M_{\tilde{q}}$ ; they are negative and of the order of  $-5\%$  in the entire range considered. As the  $g\gamma$ -channel does not contribute to LR+RL production these predictions are not affected by large photon PDF uncertainties. It is worth to notice that in LR+RL production the entire  $\mathcal{O}(\alpha_s\alpha)$  contribution is in general zero, due to the different chiralities in the final state. Moreover, the size of the  $\mathcal{O}(\alpha^2)$  contribution is negligible. Thus, in LR+RL production, the total EW corrections can be identified with the  $\mathcal{O}(\alpha_s^2\alpha)$  NLO EW corrections.

**Scan in  $M_2$ :** Results for the scan in  $M_2$  are shown in Fig. 4. The QCD corrections to the inclusive cross section are independent of  $M_2$  and of the order of 65%, while the total EW corrections are negative and small, of the order of 3%. The NLO EW corrections,  $\mathcal{O}(\alpha_s^2\alpha)$ , are negative and constant; the mild dependence on  $M_2$  is induced by the EW tree-level induced contributions. As can be inferred from Figs. 4(c)–4(f), the EW corrections do depend on the chirality of the produced squarks. In the case of LL production, they strongly depend on  $M_2$  ranging from  $-3\%$  to  $-10\%$  as  $M_2$  varies from 50 to 1200 GeV. This dependence is mainly induced by the  $\mathcal{O}(\alpha^2)$  contribution, which is suppressed for large values of  $M_2$ . Both in LL and RR production the relative contribution of the  $g\gamma$ -channel is enhanced to 10%. At variance with LL production, the EW corrections in RR production are independent of  $M_2$ , positive and of the order of 5%. As can be noticed in Fig. 4(f), for LR+RL production the only non-vanishing contribution to the total EW corrections is the  $\mathcal{O}(\alpha_s^2\alpha)$  NLO EW, which is of the order of  $-5\%$ .

**Scan in  $m_{\tilde{g}}$ :** The dependence of the QCD corrections on  $m_{\tilde{g}}$  is mild and of the order of 60% in the entire range considered, as shown in Fig. 5. The EW corrections are small, negative and of the order of  $-4\%$  in the low- $m_{\tilde{g}}$  region. They increase to  $-2.5\%$  for  $m_{\tilde{g}} \simeq 2000$  GeV. As can be inferred from Figs. 5(b), the increment is mainly due to the positive yield from the  $\mathcal{O}(\alpha^2)$  contribution and the  $g\gamma$ -channel. Again, the  $g\gamma$ -channel and the corresponding PDF uncertainty are of the same order as the EW corrections themselves. As shown in Figs. 4(c) and 4(d), the EW corrections are more important in the case of LL production. In the large  $m_{\tilde{g}}$  region, the  $\mathcal{O}(\alpha^2)$  and the  $g\gamma$ -channel contributions become dominant and render the EW corrections positive and small, of the order of 1%. As shown in Fig. 5(e) and 5(f) the total EW corrections to RR and LR+RL production are respectively of the order of  $-2\%$  and  $-5\%$  in the entire region considered. Again, in LL and RR production the photon PDF could substantially alter the size of the EW corrections, while for LR+RL production the photon PDF does not contribute.

### Non-degenerate squark masses

In the following scenarios the left- and right-handed soft squark masses  $m_{\tilde{q}_R}$  and  $m_{\tilde{q}_L}$  are treated as non-degenerate parameters. Here, NLO QCD corrections cannot be computed by `Prospino` and are not included in the analysis.

**Slope  $S_2$ :** For this scan, displayed in Fig. 6, we set  $m_{\tilde{q}_R} = 2m_{\tilde{q}_L}$ ; hence, RR production is negligible and the cross section for LR+RL is much smaller than for LL production. Therefore EW corrections to the inclusive squark–antisquark production are qualitatively very similar to the EW corrections to LL production in the slope  $S_1$ . The overall size of

the EW corrections is the result of mutual cancellations among the different channels and their dependence on  $M_{\tilde{q}}$  is mostly determined by the  $g\gamma$ -channel. Thus, the photon PDF uncertainty may substantially alter these corrections. RR production is strongly suppressed by the high mass of the produced squarks, i.e. the scan covers values of  $m_{\tilde{q}_R}$  in the range [2 TeV, 5 TeV]. In this regime, the photon PDF uncertainty renders the EW corrections to RR production unreliable. The clear sign of their unphysical behavior is the “bump” at  $M_{\tilde{q}} \equiv m_{\tilde{q}_R}/2 = 1.7$  TeV, which is due to the photon PDF and not from matrix elements.

**Slope  $S_3$ :** In this scenarios (see Fig. 7) with  $m_{\tilde{q}_L} = 2m_{\tilde{q}_R}$ , both LO predictions and higher-order corrections are mostly determined from RR production. The summed EW corrections are positive and increase as  $M_{\tilde{q}}$  increases, reaching 10% in correspondence to  $M_{\tilde{q}} \simeq 2000$  GeV. The mass hierarchy is inverted wrt. the one of the slope  $S_2$ , so the qualitative discussion for the LL(RR) contribution in  $S_2$  applies here for the RR(LL) contribution. The main difference with  $S_2$ , as can be seen from Fig. 7(e), is the fact that there are no large cancellations among the different EW contributions for RR(inclusive) production.

**Slope  $S_4$ :** In this scan (Fig. 8) the mass of the right-handed squark  $m_{\tilde{q}_R}$  is kept fix at  $m_{\tilde{q}_R} = 1.5$  TeV, while  $m_{\tilde{q}_L} = M_{\tilde{q}}$  is varied. As can be seen in the lower panel of Fig. 8(c), the hierarchy of the LO predictions for LL, RR and LR+RL depends on  $M_{\tilde{q}}$ . Consequentially, also the EW corrections and the individual perturbative orders receive the dominant contributions from LL, RR or LR+RL depending on the value of  $M_{\tilde{q}}$ . In RR production, Fig. 8(e), the EW corrections are constant by construction and corresponds to those of the spectrum in Table 2. Also the summed LR+RL production, Fig. 8(f), does not show a visible dependence on  $M_{\tilde{q}}$ . LL production shows a very similar behavior as observed for the slopes  $S_1$  and  $S_2$ .

**Slope  $S_5$ :** In this scan, referring to Fig. 9, the mass of the right-handed squark  $m_{\tilde{q}_L}$  is kept fix at  $m_{\tilde{q}_L} = 1.5$  TeV, while  $m_{\tilde{q}_R} = M_{\tilde{q}}$  is varied. Thus the LO cross sections are those of Slope  $S_4$  with LL and RR exchanged, cfr. Fig. 8(c) and Fig. 9(c). The qualitative behavior of the electroweak corrections to the different production channels can be understood as an interchange of LL with RR with respect to Slope  $S_4$ .

### 3.3 Differential distributions

In the previous subsection we studied the numerical impact of the EW corrections to the total cross section for squark–antisquark production at the LHC. It is well known that, at high energies, Sudakov-type logarithms can enhance the EW contributions. Therefore, in the following we study the impact of the EW corrections on three kinematic distributions: the transverse momentum of the produced squark, the maximal pseudo-rapidity of the squark and the anti-squark, and the invariant mass of the squark–antisquark system, defined as

$$p_T \equiv p_{T\tilde{q}_\alpha}, \quad \eta \equiv \begin{cases} \eta_{\tilde{q}_\alpha} & \text{if } |\eta_{\tilde{q}_\alpha}| \geq |\eta_{\tilde{q}_\beta^*}| \\ \eta_{\tilde{q}_\beta^*} & \text{if } |\eta_{\tilde{q}_\alpha}| < |\eta_{\tilde{q}_\beta^*}| \end{cases}, \quad M_{\text{inv}} \equiv \sqrt{(p_{\tilde{q}_\alpha} + p_{\tilde{q}_\beta^*})^2}, \quad (3.4)$$

respectively. The quantities  $p_j$ ,  $p_{Tj}$  and  $\eta_j$  denote the four-momentum, the transverse momentum and the pseudo-rapidity of the particle  $j$ . It is worth to remind that these



distributions cannot be directly observed at the experimental level; a realistic phenomenological evaluation requires the combination of the production process with the decays of the squarks. Nevertheless, it is important and useful to identify the kinematic dependence of EW corrections at the production level, before performing a complete simulation including squark decays and acceptance cuts.

For illustration of the effects, we consider, as a benchmark, the scenario defined in Table 2, but now with  $M_{\tilde{q},L} = M_{\tilde{q},R} = 2000$  GeV, i.e. a scenario within the reach of Run-II of the LHC. The numerical results for distributions in  $p_T$ ,  $\eta$  and  $M_{\text{inv}}$  are collected in Fig. 10, Fig. 11 and Fig. 12 respectively. In the left plots we always show the absolute predictions at LO with and without the EW corrections. The right plots contain the relative size of the EW corrections with respect to the LO prediction, and the breakdown to their various individual contributions. From top to bottom, the plots are arranged to display the predictions for inclusive, LL, RR, and LR+RL production. The overall behavior with respect to the different kinematic observables is strongly dependent on the chirality configuration of the produced squarks.

The EW corrections to the  $p_T$  distribution, shown in Fig. 10, are largest for the LL squark configurations, owing to their hypercharge. In particular they are negative and reach 20% and more for large  $p_T$ . The LR+RL configurations, which dominate the inclusive cross section, are influenced by  $-10\%$  for large  $p_T$ . In the RR configurations, the EW corrections always stay below 5%.

The  $\mathcal{O}(\alpha_s\alpha)$  and  $\mathcal{O}(\alpha^2)$  Born contributions, relevant only for LL and RR production, have always opposite sign and similar magnitude, resulting in mutual cancellations in most of the  $p_T$ -spectrum. The photon-induced production channel, again only relevant for LL and RR production, can yield sizable contributions both at small and at very large  $p_T$ . In particular, in the case of RR production it tends to overcompensate the negative NLO EW contribution.

Turning now to the EW corrections in the pseudo-rapidity  $\eta$  of the produced squarks (Fig. 11), the origin of the large photon-induced contributions at small  $p_T$  becomes evident. The photon induced production modes show a different angular dependence as compared to the LO prediction or the NLO EW, i.e. they are strongly enhanced in the forward region at large  $|\eta|$ , while the NLO EW corrections are mildly enhanced for small  $|\eta|$ . Due to this large dependence on  $\eta$ , the relative corrections induced by photon-induced contributions on experimental rates can strongly be affected by the details of the analysis cuts on the squark decay products.

Finally we turn to the distributions in the invariant mass of the produced squark–antisquark pair (Fig. 12). Again we observe a partial mutual cancellation between the different contributions to the EW corrections. Moreover, the NLO EW corrections are not significantly enhanced at large invariant masses.

## 4. Conclusions

In this paper we have presented the first phenomenological study of the NLO EW corrections to squark–antisquark production at the LHC including all production channels and

chirality combinations of the produced squarks.

Our analysis has shown that electroweak contributions to  $\tilde{q}_\alpha \tilde{q}_\beta^*$  production are not negligible even at the inclusive level. The  $\mathcal{O}(\alpha_s^2 \alpha)$  NLO EW contributions are negative, in general sizable and increase in relative size with the mass of the produced squarks. For the production of a left-handed squark and antisquark pair they reach  $-20\%$  for squark masses of 2 TeV. For the production of two left- or two right-handed squarks these negative contributions are typically (over-)compensated by large tree-level contributions from the photon–gluon initial state, which also increase in relative size for large masses. However, these contributions are accompanied by very large intrinsic PDF uncertainties, which may substantially alter the size of the electroweak corrections and, for large masses, the accuracy of the total predictions. The dependence on the remaining MSSM parameters is found to be very weak for the NLO EW  $\mathcal{O}(\alpha_s^2 \alpha)$  and the photon-induced contributions. The subleading Born contributions of  $\mathcal{O}(\alpha_s \alpha)$  and  $\mathcal{O}(\alpha^2)$  are not negligible and show a moderate dependence on  $m_{\tilde{g}}$  and  $M_2$ .

Besides inclusive cross sections, the electroweak corrections to squark–antisquark production are also investigated at the differential level. The  $\mathcal{O}(\alpha_s^2 \alpha)$  NLO EW corrections show a typical Sudakov behavior, i.e. increasing influence at large transverse momenta of the produced squarks. As on the inclusive level, these corrections are partly compensated by large contributions from photon-induced production. The origin of these large contributions can clearly be attributed to a qualitatively different behavior of the photon-induced channels at large pseudo-rapidities.

In general, in studies for squark production as well as in corresponding data analyses, when EW effects are usually neglected for reasons of simplicity, the size of the EW contributions calculated and visualized in this paper, can serve as an estimate of the uncertainty of the theoretical predictions, on top of the uncertainty resulting from the QCD side.

## Acknowledgments

We are grateful to S. Carrazza and J. Rojo for clarifications concerning NNPDF2.3QED. JML was supported by the European Commission through the “LHCPhenoNet” Initial Training Network PITN-GA-2010-264564. DP was supported by the the ERC grant 291377 “LHCtheory: Theoretical predictions and analyses of LHC physics: advancing the precision frontier”. This research was supported by the Munich Institute for Astro- and Particle Physics (MIAPP) of the DFG cluster of excellence “Origin and Structure of the Universe”.

## References

- [1] J. Wess and B. Zumino, *Supergauge Transformations in Four-Dimensions*, *Nucl. Phys.* **B70** (1974) 39–50.
- [2] H. P. Nilles, *Supersymmetry, Supergravity and Particle Physics*, *Phys. Rept.* **110** (1984) 1–162.
- [3] H. E. Haber and G. L. Kane, *The Search for Supersymmetry: probing physics beyond the Standard Model*, *Phys. Rept.* **117** (1985) 75–263.

- [4] R. Barbieri, *Looking beyond the Standard Model: the Supersymmetric Option*, *Riv. Nuovo Cim.* **11N4** (1988) 1–45.
- [5] **ATLAS** Collaboration, G. Aad *et. al.*, *Observation of a new particle in the search for the Standard Model Higgs boson with the ATLAS detector at the LHC*, *Phys.Lett.* **B716** (2012) 1–29, [[arXiv:1207.7214](https://arxiv.org/abs/1207.7214)].
- [6] **CMS** Collaboration, S. Chatrchyan *et. al.*, *Observation of a new boson at a mass of 125 GeV with the CMS experiment at the LHC*, *Phys.Lett.* **B716** (2012) 30–61, [[arXiv:1207.7235](https://arxiv.org/abs/1207.7235)].
- [7] **ATLAS** Collaboration. ATLAS Supersymmetry (SUSY) searches page: <https://twiki.cern.ch/twiki/bin/view/AtlasPublic/SupersymmetryPublicResults>.
- [8] **CMS** Collaboration. CMS Supersymmetry Physics Results page: <https://twiki.cern.ch/twiki/bin/view/CMSPublic/PhysicsResultsSUS>.
- [9] G. L. Kane and J. P. Leveille, *Experimental constraints on gluino masses and supersymmetric theories*, *Phys. Lett.* **B112** (1982) 227.
- [10] P. R. Harrison and C. H. Llewellyn Smith, *Hadroproduction of supersymmetric particles*, *Nucl. Phys.* **B213** (1983) 223.
- [11] E. Reya and D. P. Roy, *Supersymmetric particle production at  $p\bar{p}$  collider energies*, *Phys. Rev.* **D32** (1985) 645.
- [12] S. Dawson, E. Eichten, and C. Quigg, *Search for supersymmetric particles in hadron–hadron collisions*, *Phys. Rev.* **D31** (1985) 1581.
- [13] H. Baer and X. Tata, *Component formulae for hadroproduction of left-handed and right-handed squarks*, *Phys. Lett.* **B160** (1985) 159.
- [14] W. Beenakker, R. Hopker, M. Spira, and P. M. Zerwas, *Squark production at the Tevatron*, *Phys. Rev. Lett.* **74** (1995) 2905–2908, [[hep-ph/9412272](https://arxiv.org/abs/hep-ph/9412272)].
- [15] W. Beenakker, R. Hopker, M. Spira, and P. M. Zerwas, *Gluino pair production at the Tevatron*, *Z. Phys.* **C69** (1995) 163–166, [[hep-ph/9505416](https://arxiv.org/abs/hep-ph/9505416)].
- [16] W. Beenakker, R. Hopker, M. Spira, and P. M. Zerwas, *Squark and gluino production at hadron colliders*, *Nucl. Phys.* **B492** (1997) 51–103, [[hep-ph/9610490](https://arxiv.org/abs/hep-ph/9610490)].
- [17] W. Beenakker, M. Krämer, T. Plehn, M. Spira, and P. M. Zerwas, *Stop production at hadron colliders*, *Nucl. Phys.* **B515** (1998) 3–14, [[hep-ph/9710451](https://arxiv.org/abs/hep-ph/9710451)].
- [18] W. Hollik, J. M. Lindert, and D. Pagani, *NLO corrections to squark-squark production and decay at the LHC*, *JHEP* **1303** (2013) 139, [[arXiv:1207.1071](https://arxiv.org/abs/1207.1071)].
- [19] D. Goncalves-Netto, D. Lopez-Val, K. Mawatari, T. Plehn, and I. Wigmore, *Automated squark and gluino production to next-to-leading order*, *Phys.Rev.* **D87** (2013) 014002, [[arXiv:1211.0286](https://arxiv.org/abs/1211.0286)].
- [20] D. Goncalves, D. Lopez-Val, K. Mawatari, and T. Plehn, *Automated third generation squark production to next-to-leading order*, [arXiv:1407.4302](https://arxiv.org/abs/1407.4302).
- [21] G. Bozzi, B. Fuks, and M. Klasen, *Non-diagonal and mixed squark production at hadron colliders*, *Phys. Rev.* **D72** (2005) 035016, [[hep-ph/0507073](https://arxiv.org/abs/hep-ph/0507073)].
- [22] A. T. Alan, K. Cankocak, and D. A. Demir, *Squark pair production in the MSSM with explicit CP violation*, *Phys. Rev.* **D75** (2007) 095002, [[hep-ph/0702289](https://arxiv.org/abs/hep-ph/0702289)].

- [23] W. Hollik, M. Kollar, and M. K. Trenkel, *Hadronic production of top-squark pairs with electroweak NLO contributions*, *JHEP* **02** (2008) 018, [[arXiv:0712.0287](#)].
- [24] S. Bornhauser, M. Drees, H. K. Dreiner, and J. S. Kim, *Electroweak contributions to squark pair production at the LHC*, *Phys. Rev.* **D76** (2007) 095020, [[arXiv:0709.2544](#)].
- [25] M. Beccaria, G. Macorini, L. Panizzi, F. M. Renard, and C. Verzegnassi, *Stop-antistop and sbottom-antisbottom production at LHC: a one-loop search for model parameters dependence*, *Int. J. Mod. Phys.* **A23** (2008) 4779–4810, [[arXiv:0804.1252](#)].
- [26] W. Hollik and E. Mirabella, *Squark anti-squark pair production at the LHC: the electroweak contribution*, *JHEP* **12** (2008) 087, [[arXiv:0806.1433](#)].
- [27] W. Hollik, E. Mirabella, and M. K. Trenkel, *Electroweak contributions to squark-gluino production at the LHC*, *JHEP* **02** (2009) 002, [[arXiv:0810.1044](#)].
- [28] S. Bornhauser, M. Drees, H. K. Dreiner, and J. S. Kim, *Rapidity gap events in squark pair production at the LHC*, *Phys. Rev.* **D80** (2009) 095007, [[arXiv:0909.2595](#)].
- [29] E. Mirabella, *NLO electroweak contributions to gluino pair production at hadron colliders*, *JHEP* **12** (2009) 012, [[arXiv:0908.3318](#)].
- [30] A. Arhrib, R. Benbrik, K. Cheung, and T.-C. Yuan, *Higgs boson enhancement effects on squark-pair production at the LHC*, *JHEP* **02** (2010) 048, [[arXiv:0911.1820](#)].
- [31] J. Germer, W. Hollik, E. Mirabella, and M. K. Trenkel, *Hadronic production of squark-squark pairs: the electroweak contributions*, *JHEP* **08** (2010) 023, [[arXiv:1004.2621](#)].
- [32] J. Germer, W. Hollik, and E. Mirabella, *Hadronic production of bottom-squark pairs with electroweak contributions*, *JHEP* **1105** (2011) 068, [[arXiv:1103.1258](#)].
- [33] J. Germer, W. Hollik, J. M. Lindert, and E. Mirabella, *Top-squark pair production at the LHC: a complete analysis at next-to-leading order*, *JHEP* **1409** (2014) 022, [[arXiv:1404.5572](#)].
- [34] U. Langenfeld and S.-O. Moch, *Higher-order soft corrections to squark hadro- production*, *Phys. Lett.* **B675** (2009) 210–221, [[arXiv:0901.0802](#)].
- [35] U. Langenfeld, *Threshold improved QCD corrections for stop-anti-stop production at hadron colliders*, *JHEP* **1107** (2011) 052, [[arXiv:1011.3341](#)].
- [36] U. Langenfeld, S.-O. Moch, and T. Pfoh, *QCD threshold corrections for gluino pair production at hadron colliders*, *JHEP* **1211** (2012) 070, [[arXiv:1208.4281](#)].
- [37] A. Broggio, A. Ferroglia, M. Neubert, L. Vernazza, and L. L. Yang, *Approximate NNLO predictions for the stop-pair production cross section at the LHC*, *JHEP* **1307** (2013) 042, [[arXiv:1304.2411](#)].
- [38] A. Kulesza and L. Motyka, *Threshold resummation for squark-antisquark and gluino- pair production at the LHC*, *Phys. Rev. Lett.* **102** (2009) 111802, [[arXiv:0807.2405](#)].
- [39] A. Kulesza and L. Motyka, *Soft gluon resummation for the production of gluino-gluino and squark-antisquark pairs at the LHC*, *Phys. Rev.* **D80** (2009) 095004, [[arXiv:0905.4749](#)].
- [40] W. Beenakker *et. al.*, *Soft-gluon resummation for squark and gluino hadroproduction*, *JHEP* **12** (2009) 041, [[arXiv:0909.4418](#)].
- [41] W. Beenakker *et. al.*, *Supersymmetric top and bottom squark production at hadron colliders*, *JHEP* **08** (2010) 098, [[arXiv:1006.4771](#)].

- [42] W. Beenakker, S. Brensing, M. Krämer, A. Kulesza, E. Laenen, *et. al.*, *Squark and gluino hadroproduction*, *Int.J.Mod.Phys.* **A26** (2011) 2637–2664, [[arXiv:1105.1110](#)].
- [43] W. Beenakker, S. Brensing, M. Krämer, A. Kulesza, E. Laenen, *et. al.*, *NNLL resummation for squark-antisquark pair production at the LHC*, *JHEP* **1201** (2012) 076, [[arXiv:1110.2446](#)].
- [44] A. Broggio, A. Ferroglia, M. Neubert, L. Vernazza, and L. L. Yang, *NNLL Momentum-Space Resummation for Stop-Pair Production at the LHC*, *JHEP* **1403** (2014) 066, [[arXiv:1312.4540](#)].
- [45] T. Pfoh, *Phenomenology of QCD threshold resummation for gluino pair production at NNLL*, *JHEP* **1305** (2013) 044, [[arXiv:1302.7202](#)].
- [46] W. Beenakker, T. Janssen, S. Lepoeter, M. Krämer, A. Kulesza, *et. al.*, *Towards NNLL resummation: hard matching coefficients for squark and gluino hadroproduction*, *JHEP* **1310** (2013) 120, [[arXiv:1304.6354](#)].
- [47] W. Beenakker, C. Borschensky, M. Krämer, A. Kulesza, E. Laenen, *et. al.*, *NNLL resummation for squark and gluino production at the LHC*, [arXiv:1404.3134](#).
- [48] M. Beneke, P. Falgari, and C. Schwinn, *Colour structure in threshold resummation and squark-antisquark production at NLL*, *PoS EPS-HEP2009* (2009) 319, [[arXiv:0909.3488](#)].
- [49] M. Beneke, P. Falgari, and C. Schwinn, *Threshold resummation for pair production of coloured heavy (s)particles at hadron colliders*, *Nucl. Phys.* **B842** (2010) [[arXiv:1007.5414](#)].
- [50] P. Falgari, C. Schwinn, and C. Wever, *NLL soft and Coulomb resummation for squark and gluino production at the LHC*, *JHEP* **1206** (2012) 052, [[arXiv:1202.2260](#)].
- [51] P. Falgari, C. Schwinn, and C. Wever, *Finite-width effects on threshold corrections to squark and gluino production*, *JHEP* **1301** (2013) 085, [[arXiv:1211.3408](#)].
- [52] M. R. Kauth, J. H. Kuhn, P. Marquard, and M. Steinhauser, *Gluinonia: energy levels, production and decay*, *Nucl.Phys.* **B831** (2010) 285–305, [[arXiv:0910.2612](#)].
- [53] C. Kim, A. Idilbi, T. Mehen, and Y. W. Yoon, *Production of stoponium at the LHC*, [arXiv:1401.1284](#).
- [54] K. Hagiwara and H. Yokoya, *Bound-state effects on gluino-pair production at hadron colliders*, *JHEP* **0910** (2009) 049, [[arXiv:0909.3204](#)].
- [55] M. R. Kauth, J. H. Kuhn, P. Marquard, and M. Steinhauser, *Gluino pair production at the LHC: the threshold*, *Nucl.Phys.* **B857** (2012) 28–64, [[arXiv:1108.0361](#)].
- [56] M. R. Kauth, A. Kress, and J. H. Kuhn, *Gluino-squark production at the LHC: the threshold*, *JHEP* **1112** (2011) 104, [[arXiv:1108.0542](#)].
- [57] W. Beenakker, R. Hopker, and P. Zerwas, *SUSY QCD decays of squarks and gluinos*, *Phys.Lett.* **B378** (1996) 159–166, [[hep-ph/9602378](#)].
- [58] A. Djouadi, W. Hollik, and C. Junger, *QCD corrections to scalar quark decays*, *Phys.Rev.* **D55** (1997) 6975–6985, [[hep-ph/9609419](#)].
- [59] W. Beenakker, R. Hopker, T. Plehn, and P. M. Zerwas, *Stop decays in SUSY-QCD*, *Z. Phys.* **C75** (1997) 349–356, [[hep-ph/9610313](#)].
- [60] J. Guasch, W. Hollik, and J. Sola, *Full electroweak one loop radiative corrections to squark decays in the MSSM*, *Phys.Lett.* **B510** (2001) 211–220, [[hep-ph/0101086](#)].

- [61] J. Guasch, W. Hollik, and J. Sola, *Fermionic decays of sfermions: a complete discussion at one loop order*, *JHEP* **0210** (2002) 040, [[hep-ph/0207364](#)].
- [62] W. Hollik, J. M. Lindert, and D. Pagani, *On cascade decays of squarks at the LHC in NLO QCD*, *Eur.Phys.J.* **C73** (2013) 2410, [[arXiv:1303.0186](#)].
- [63] R. Boughezal and M. Schulze, *Precise predictions for top-quark plus missing energy signatures at the LHC*, *Phys.Rev.Lett.* **110** (2013), no. 19 192002, [[arXiv:1212.0898](#)].
- [64] R. Boughezal and M. Schulze,  *$t\bar{t}$ +large missing energy from top-quark partners: a comprehensive study at next-to-leading order QCD*, *Phys.Rev.* **D88** (2013), no. 11 114002, [[arXiv:1309.2316](#)].
- [65] R. Gavin, C. Hangst, M. Krämer, M. Muhlleitner, M. Pellen, *et. al.*, *Matching squark pair production at NLO with parton showers*, *JHEP* **10** (2013) 187, [[arXiv:1305.4061](#)].
- [66] R. Gavin, C. Hangst, M. Krmer, M. Mhlleitner, M. Pellen, *et. al.*, *Squark Production and Decay matched with Parton Showers at NLO*, [arXiv:1407.7971](#).
- [67] **ATLAS** Collaboration, G. Aad *et. al.*, *Search for squarks and gluinos with the ATLAS detector in final states with jets and missing transverse momentum using  $\sqrt{s} = 8$  TeV proton–proton collision data*, *JHEP* **1409** (2014) 176, [[arXiv:1405.7875](#)].
- [68] M. Krämer, A. Kulesza, R. van der Leeuw, M. Mangano, S. Padhi, *et. al.*, *Supersymmetry production cross sections in pp collisions at  $\sqrt{s} = 7$  TeV*, [arXiv:1206.2892](#).
- [69] W. Beenakker, R. Hopker, and M. Spira, *PROSPINO: A program for the PROduction of Supersymmetric Particles In Next-to-leading Order QCD*, [hep-ph/9611232](#).
- [70] J. Alwall, R. Frederix, S. Frixione, V. Hirschi, F. Maltoni, *et. al.*, *The automated computation of tree-level and next-to-leading order differential cross sections, and their matching to parton shower simulations*, *JHEP* **1407** (2014) 079, [[arXiv:1405.0301](#)].
- [71] T. Hahn, *Generating Feynman diagrams and amplitudes with FeynArts 3*, *Comput. Phys. Commun.* **140** (2001) 418–431, [[hep-ph/0012260](#)].
- [72] T. Hahn and M. Rauch, *News from FormCalc and LoopTools*, *Nucl. Phys. Proc. Suppl.* **157** (2006) 236–240, [[hep-ph/0601248](#)].
- [73] T. Hahn and C. Schappacher, *The implementation of the minimal supersymmetric standard model in FeynArts and FormCalc*, *Comput. Phys. Commun.* **143** (2002) 54–68, [[hep-ph/0105349](#)].
- [74] D. R. Yennie, S. C. Frautschi, and H. Suura, *The infrared divergence phenomena and high-energy processes*, *Ann. Phys.* **13** (1961) 379–452.
- [75] S. Weinberg, *Infrared photons and gravitons*, *Phys. Rev.* **140** (1965) B516–B524.
- [76] V. N. Baier, V. S. Fadin, and V. A. Khoze, *Quasireal electron method in high-energy quantum electrodynamics*, *Nucl. Phys.* **B65** (1973) 381–396.
- [77] **NNPDF** Collaboration, R. D. Ball *et. al.*, *Parton distributions with QED corrections*, *Nucl.Phys.* **B877** (2013), no. 2 290–320, [[arXiv:1308.0598](#)].
- [78] **NNPDF** Collaboration, C. S. Deans, *Progress in the NNPDF global analysis*, [arXiv:1304.2781](#).
- [79] **NNPDF** Collaboration, R. D. Ball *et. al.*, *Parton distributions for the LHC Run II*, [arXiv:1410.8849](#).

- [80] **Particle Data Group** Collaboration, K. Olive *et. al.*, *Review of Particle Physics*, *Chin.Phys.* **C38** (2014) 090001.
- [81] S. Heinemeyer, W. Hollik, and G. Weiglein, *The masses of the neutral CP - even Higgs bosons in the MSSM: accurate analysis at the two loop level*, *Eur.Phys.J.* **C9** (1999) 343–366, [[hep-ph/9812472](#)].
- [82] S. Heinemeyer, W. Hollik, and G. Weiglein, *FeynHiggs: a program for the calculation of the masses of the neutral CP-even Higgs bosons in the MSSM*, *Comput. Phys. Commun.* **124** (2000) 76–89, [[hep-ph/9812320](#)].
- [83] M. Frank *et. al.*, *The Higgs boson masses and mixings of the complex MSSM in the Feynman-diagrammatic approach*, *JHEP* **02** (2007) 047, [[hep-ph/0611326](#)].
- [84] T. Hahn, S. Heinemeyer, W. Hollik, H. Rzehak, and G. Weiglein, *FeynHiggs: A program for the calculation of MSSM Higgs-boson observables - version 2.6.5*, *Comput.Phys.Commun.* **180** (2009) 1426–1427.
- [85] T. Hahn, S. Heinemeyer, W. Hollik, H. Rzehak, and G. Weiglein, *High-precision predictions for the light CP-even Higgs Boson Mass of the MSSM*, [arXiv:1312.4937](#).
- [86] R. Boughezal, Y. Li, and F. Petriello, *Disentangling radiative corrections using the high-mass Drell-Yan process at the LHC*, *Phys.Rev.* **D89** (2014), no. 3 034030, [[arXiv:1312.3972](#)].
- [87] S. Carrazza, *Disentangling electroweak effects in Z-boson production*, [arXiv:1405.1728](#).
- [88] *Search for Supersymmetry at the high luminosity LHC with the ATLAS experiment*, Tech. Rep. ATL-PHYS-PUB-2014-010, CERN, Geneva, Jul, 2014.
- [89] M. Carena, S. Heinemeyer, O. Stål, C. Wagner, and G. Weiglein, *MSSM Higgs boson searches at the LHC: benchmark scenarios after the discovery of a Higgs-like particle*, *Eur. Phys. J.* **C73** (2013) 2552, [[arXiv:1302.7033](#)].
- [90] P. Bechtle, O. Brein, S. Heinemeyer, G. Weiglein, and K. E. Williams, *HiggsBounds: confronting arbitrary Higgs sectors with exclusion bounds from LEP and the Tevatron*, *Comput.Phys.Commun.* **181** (2010) 138–167, [[arXiv:0811.4169](#)].
- [91] P. Bechtle, O. Brein, S. Heinemeyer, G. Weiglein, and K. E. Williams, *HiggsBounds 2.0.0: confronting neutral and charged Higgs sector predictions with exclusion bounds from LEP and the Tevatron*, *Comput.Phys.Commun.* **182** (2011) 2605–2631, [[arXiv:1102.1898](#)].
- [92] P. Bechtle, O. Brein, S. Heinemeyer, O. Stål, T. Stefaniak, *et. al.*, *Recent developments in HiggsBounds and a preview of HiggsSignals*, *PoS CHARGED2012* (2012) 024, [[arXiv:1301.2345](#)].
- [93] P. Bechtle, O. Brein, S. Heinemeyer, O. Stål, T. Stefaniak, *et. al.*, *HiggsBounds-4: improved tests of extended Higgs sectors against exclusion bounds from LEP, the Tevatron and the LHC*, *Eur.Phys.J.* **C74** (2014) 2693, [[arXiv:1311.0055](#)].
- [94] P. Bechtle, S. Heinemeyer, O. Stål, T. Stefaniak, and G. Weiglein, *HiggsSignals: confronting arbitrary Higgs sectors with measurements at the Tevatron and the LHC*, *Eur.Phys.J.* **C74** (2014) 2711, [[arXiv:1305.1933](#)].

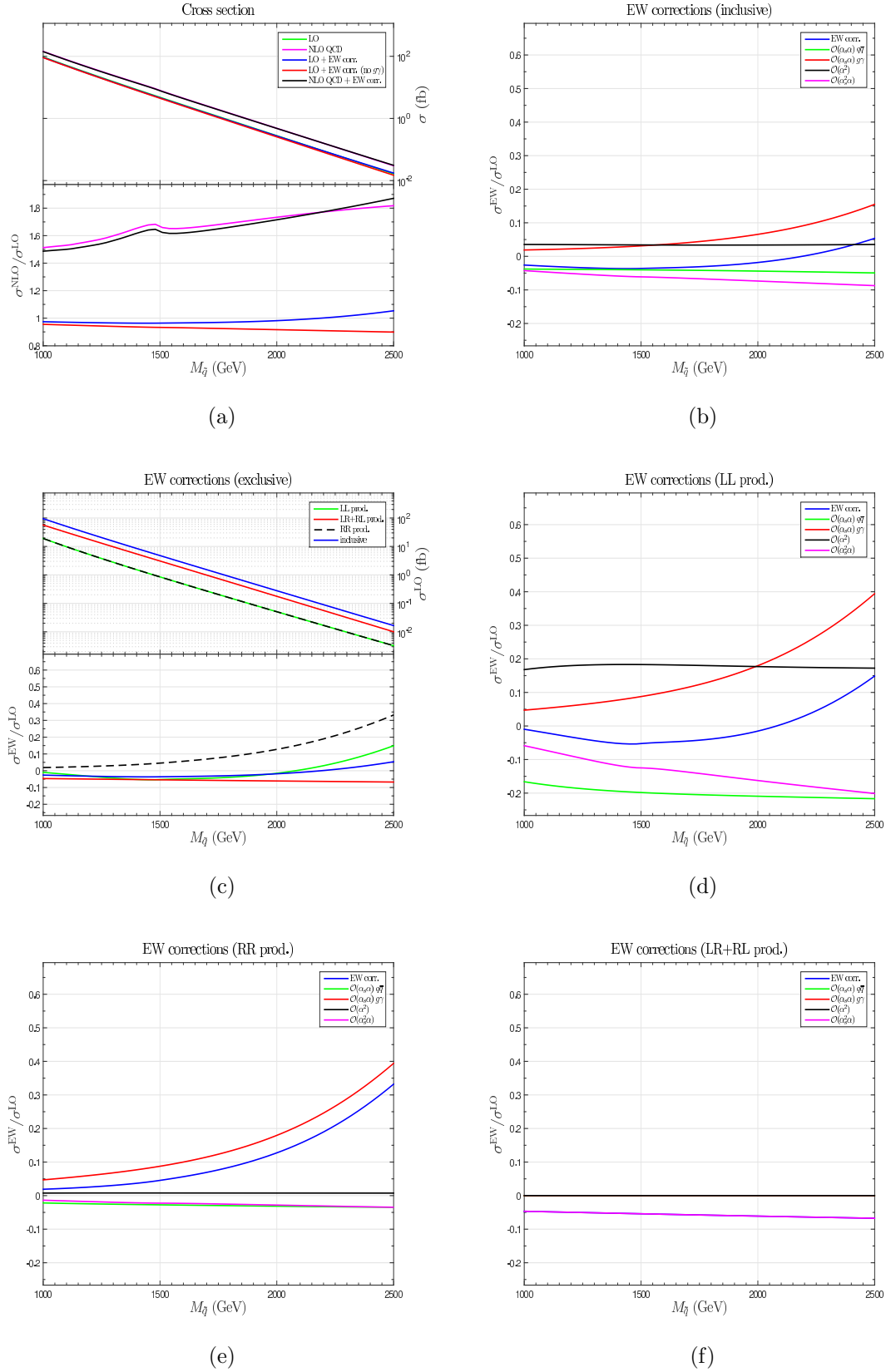


Figure 3: Scan over  $M_{\bar{q}}$ , which corresponds to Slope  $S_1$ . The value of the other parameters are collected in Table 2.



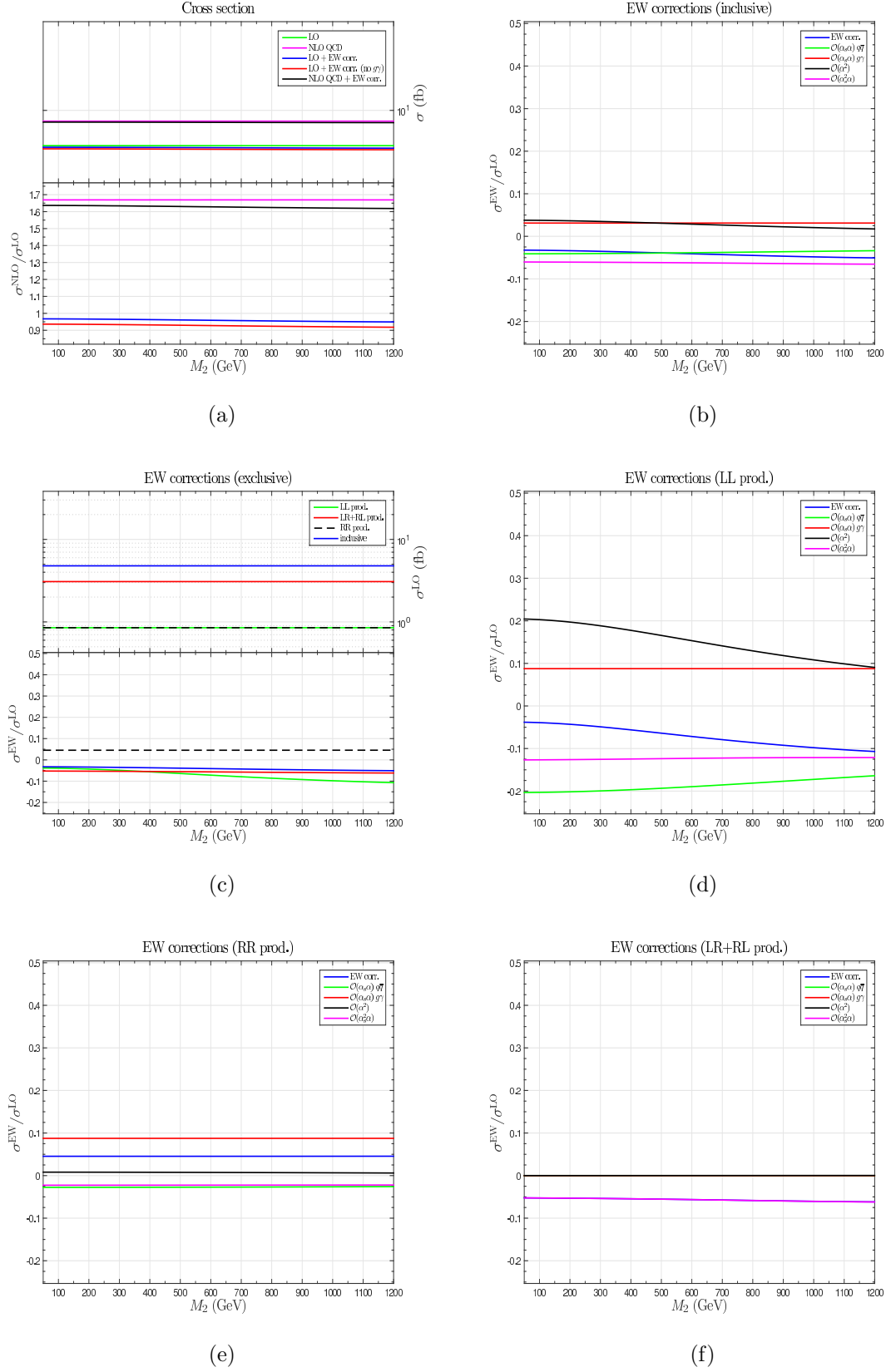


Figure 4: Scan over  $M_2$ . The value of the other parameters are collected in Table 2.

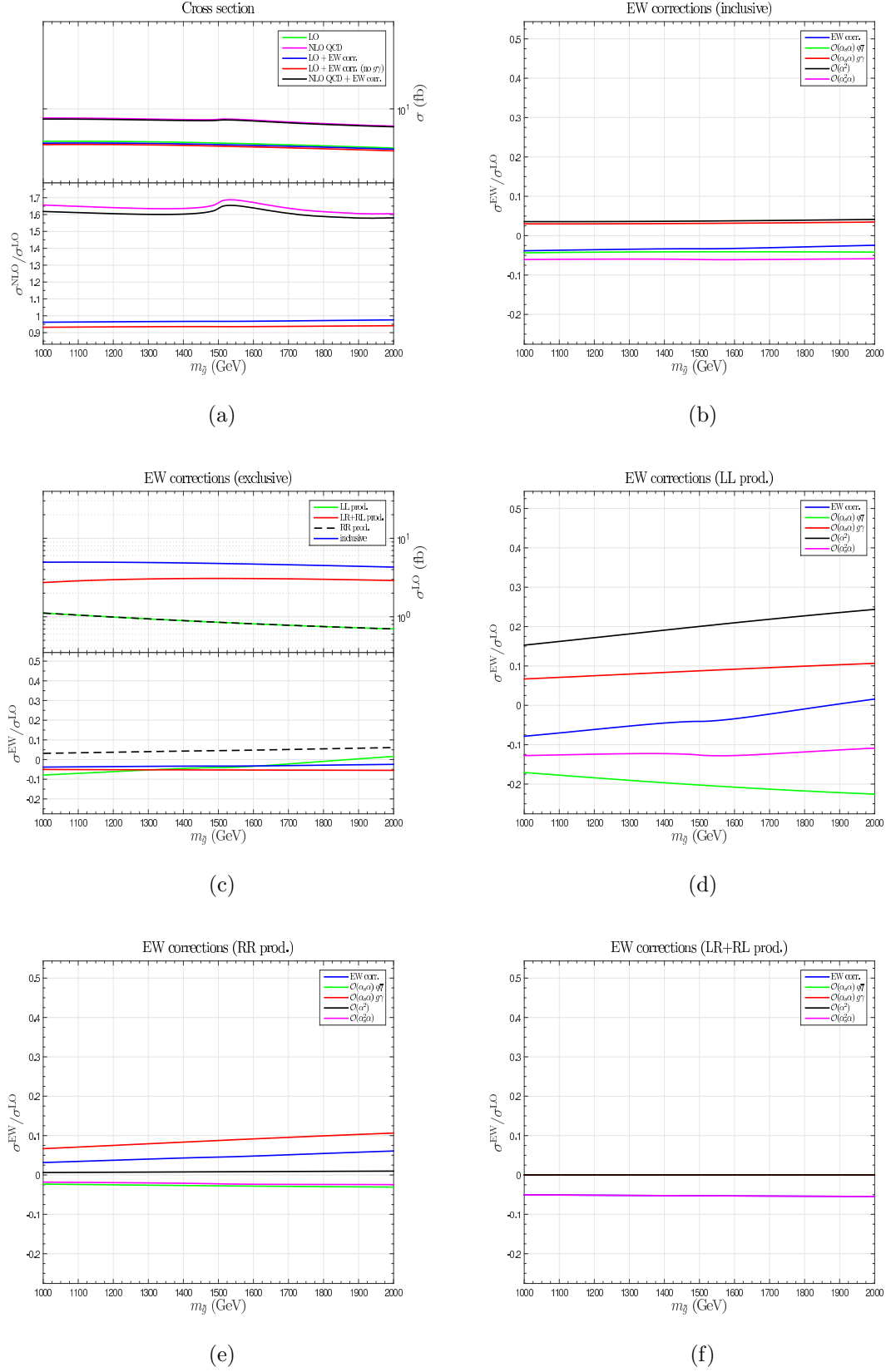


Figure 5: Scan over  $m_{\tilde{g}}$ . The value of the other parameters are collected in Table 2.

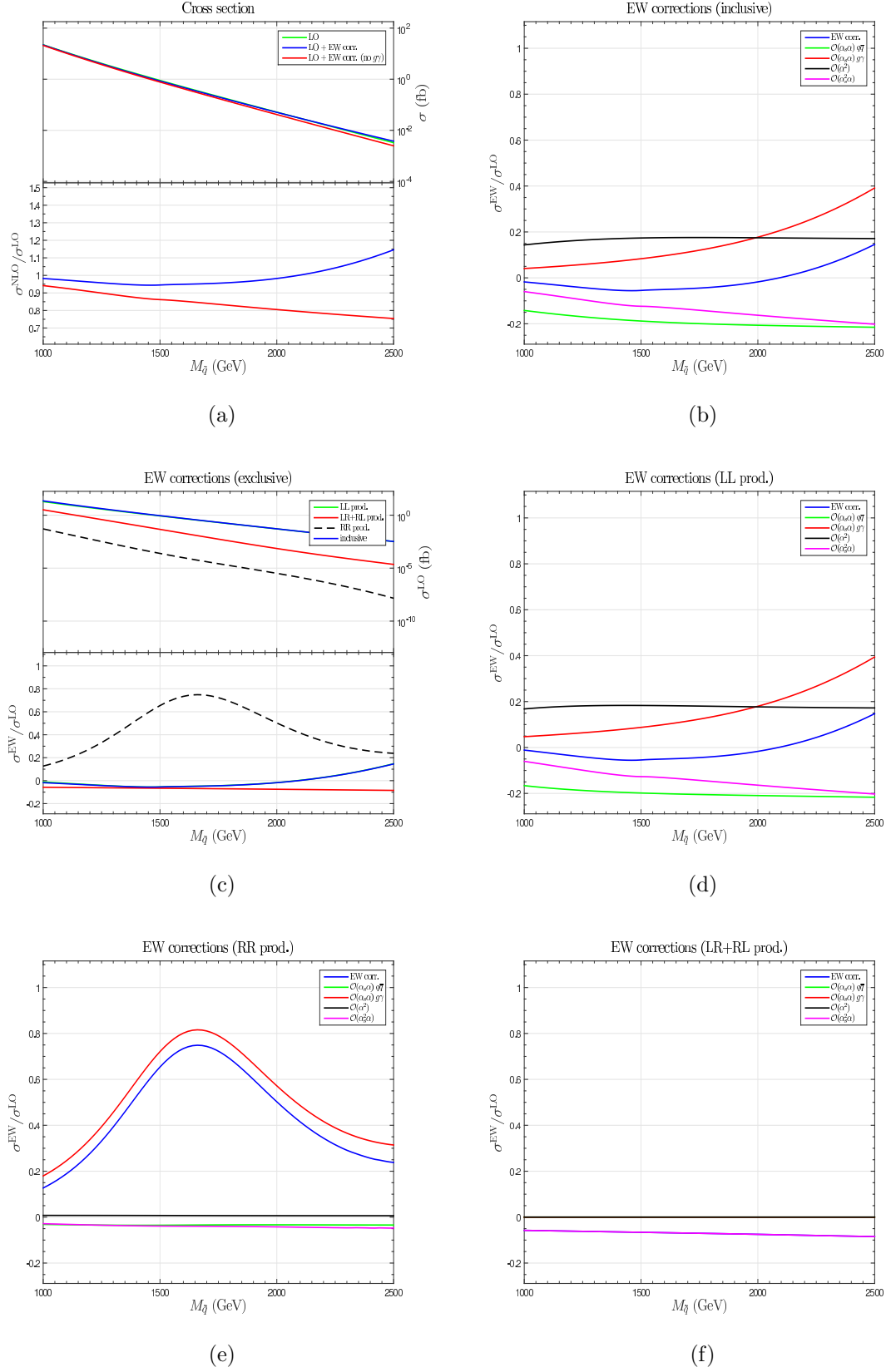


Figure 6: Slope  $S_2$ : scan over  $M_{\tilde{q}}$ . The value of the parameters not involved in the scan are collected in Table 2.

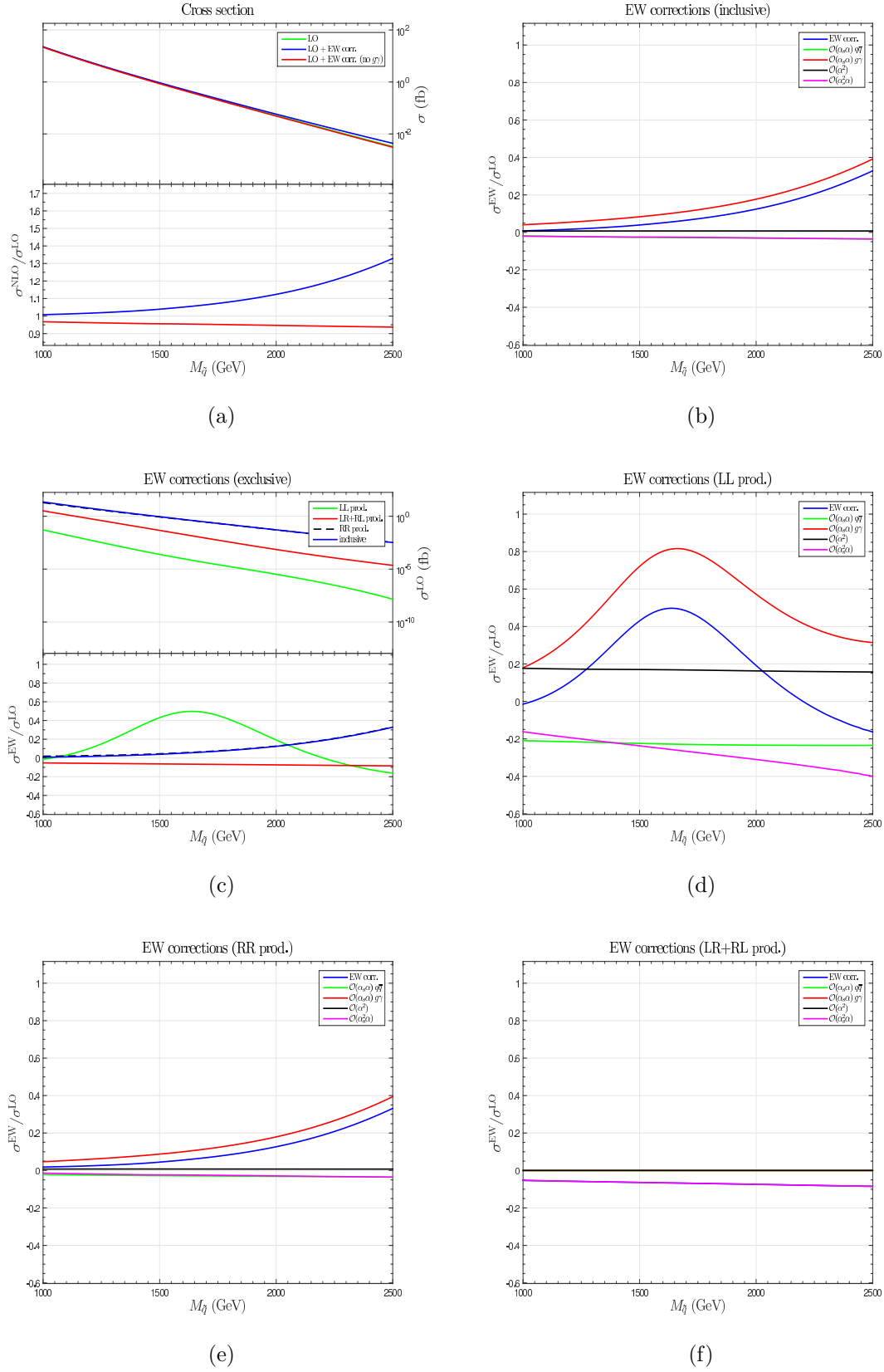


Figure 7: Slope  $S_3$ : scan over  $M_{\tilde{q}}$ . The value of the parameters not involved in the scan are collected in Table 2.

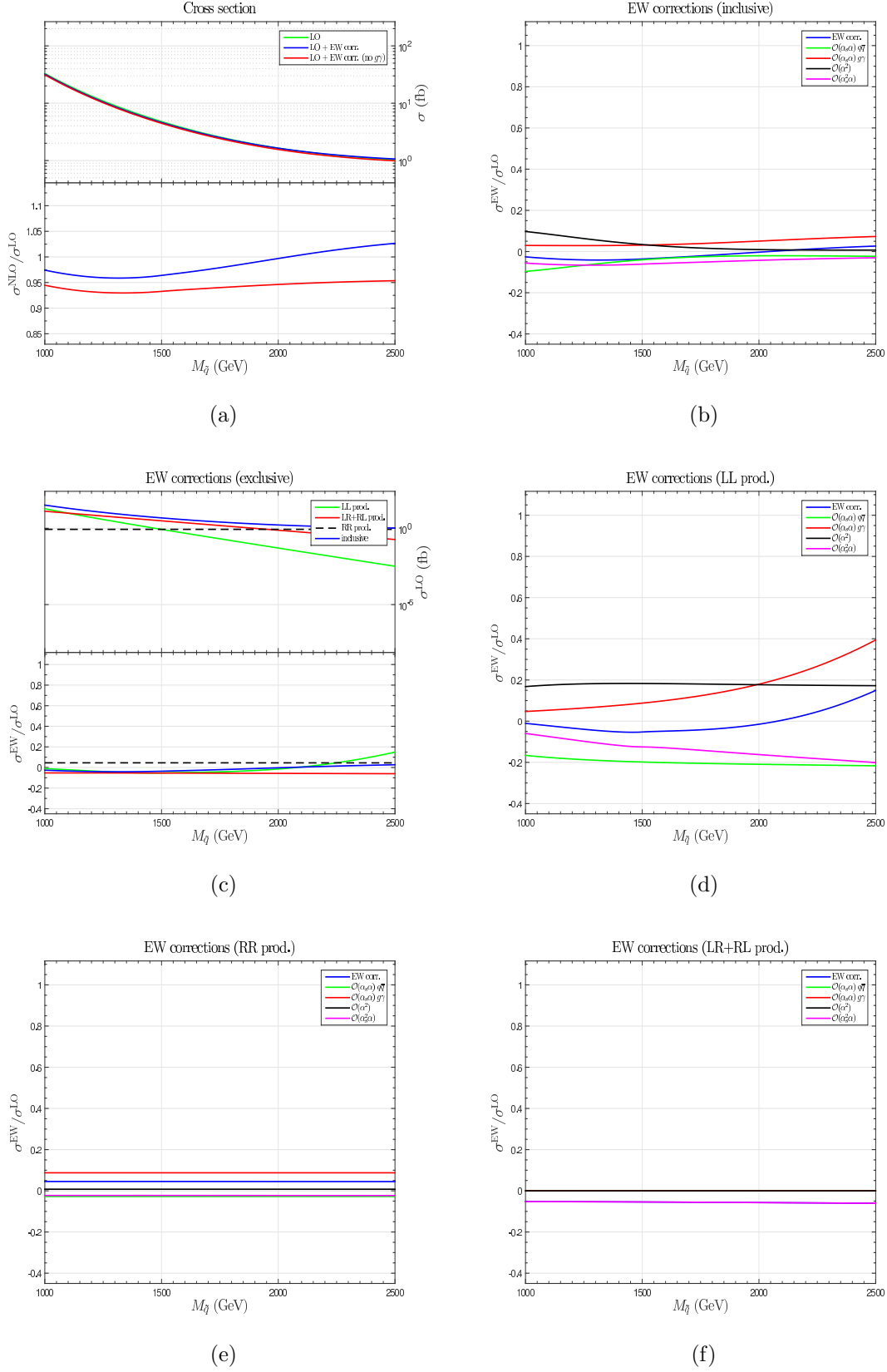


Figure 8: Slope  $S_4$ : scan over  $M_{\bar{q}}$ . The value of the parameters not involved in the scan are collected in Table 2.

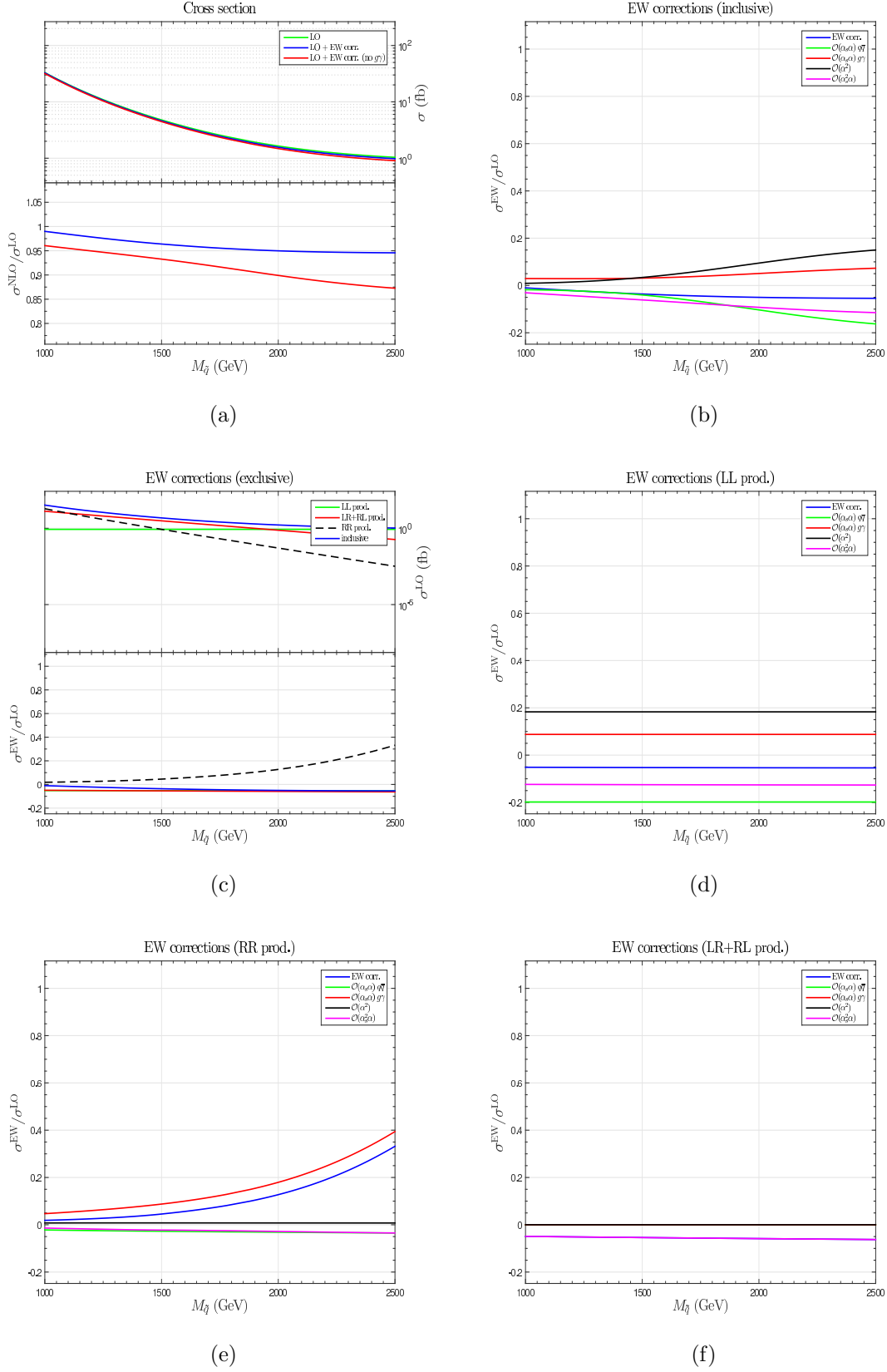


Figure 9: Slope  $S_5$ : scan over  $M_{\bar{q}}$ . The value of the parameters not involved in the scan are collected in Table 2.

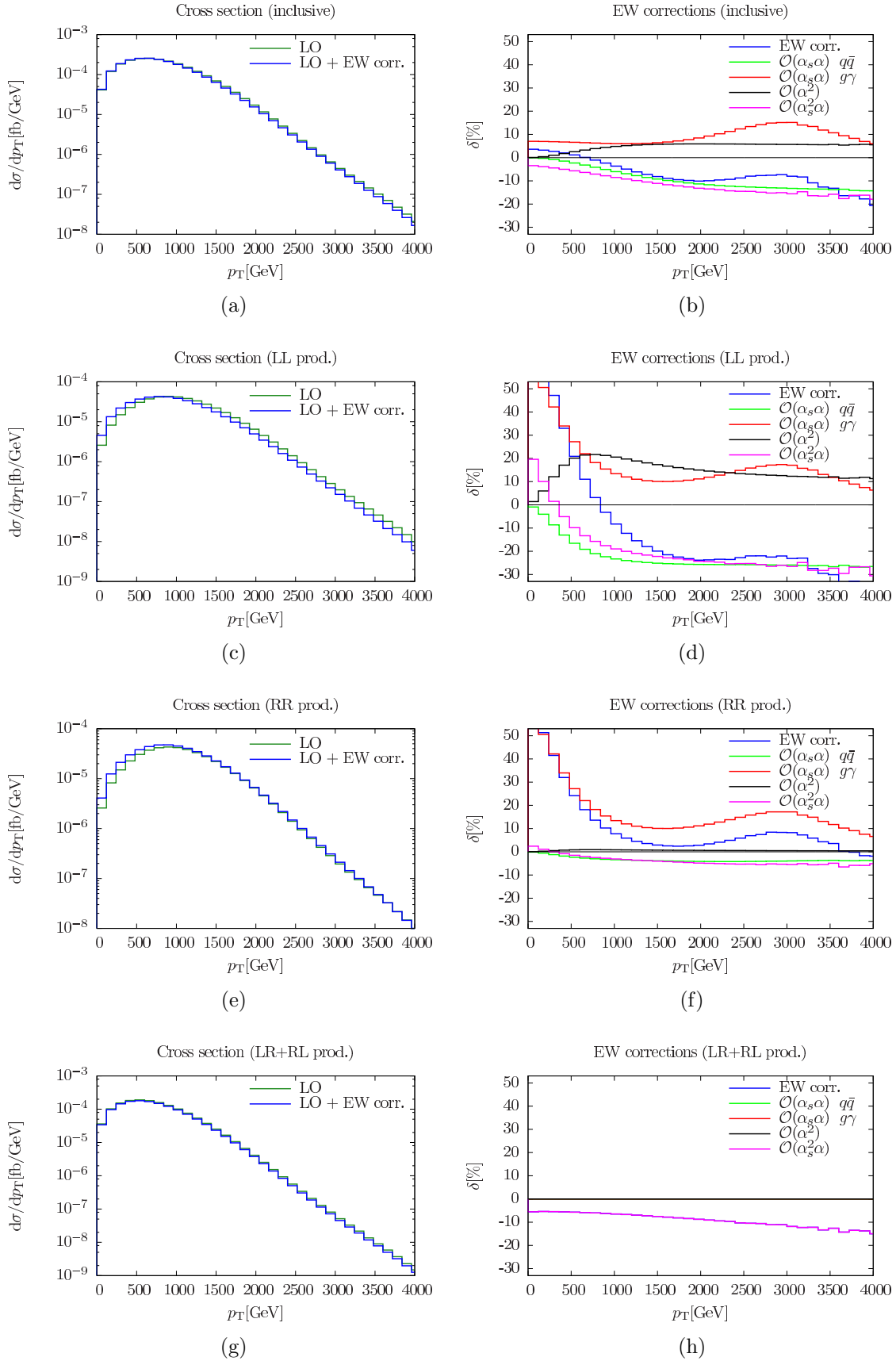


Figure 10: Differential distributions in the transverse momentum  $p_T$  of the produced squark.

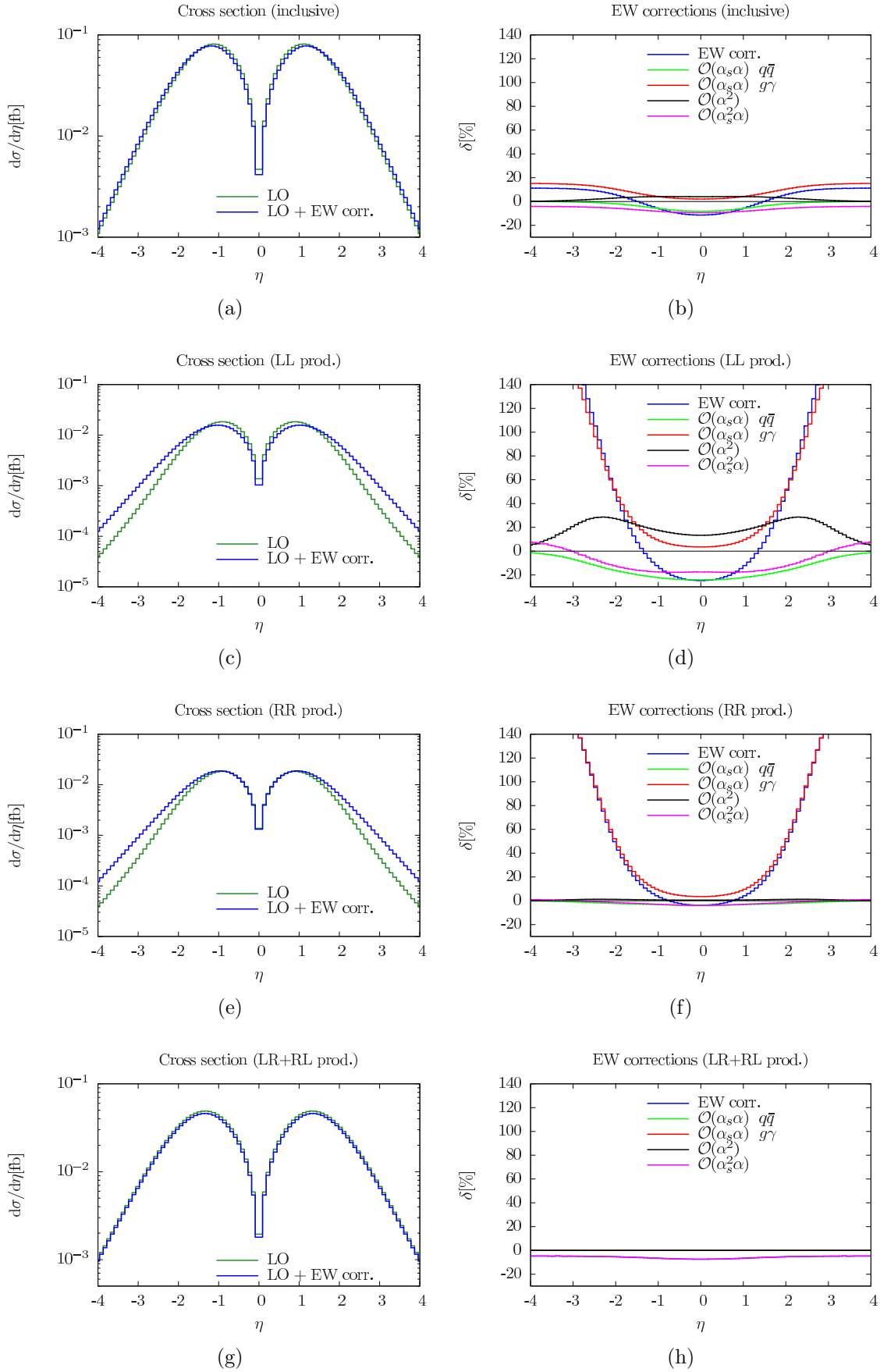


Figure 11: Differential distributions in the maximal pseudorapidity  $\eta$  of the produced squarks, as defined in eq. (3.4). – 31 –



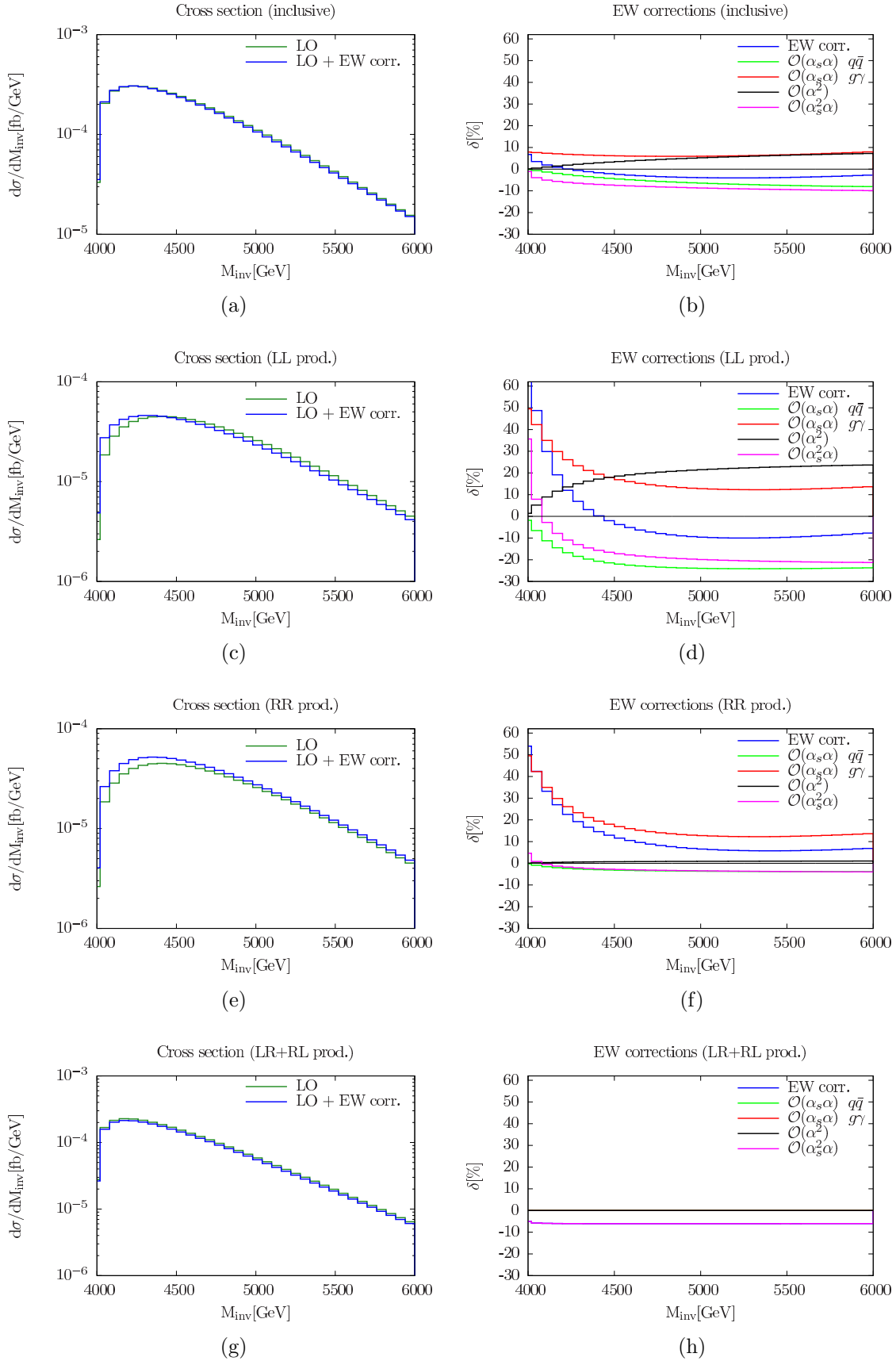


Figure 12: Differential distributions in the invariant mass  $M_{\text{inv}}$  of the produced squark-anti-squark pair.